Bergische Universität Wuppertal

Fachbereich Mathematik und Naturwissenschaften

Lehrstuhl für Angewandte Mathematik
und Numerische Mathematik

Lehrstuhl für Optimierung und Approximation

Preprint BUW-AMNA-OPAP 10/04

Xavier Antoine, Christophe Besse, Matthias Ehrhardt
and Pauline Klein

Modeling boundary conditions for solving stationary Schrödinger equations

February 2010

http://www.math.uni-wuppertal.de

Modeling boundary conditions for solving stationary Schrödinger equations

Xavier Antoine[a,1,*], Christophe Besse[b,1], Matthias Ehrhardt[c], Pauline Klein[a,1]

[a] *Institut Elie Cartan Nancy, Nancy-Université, CNRS UMR 7502, INRIA CORIDA Team, Boulevard des Aiguillettes B.P. 239, 54506 Vandoeuvre-lès-Nancy, France*
[b] *Laboratoire Paul Painlevé, CNRS UMR 8524, Simpaf Project Team - Inria CR Lille Nord Europe, Université des Sciences et Technologies de Lille, Cité Scientifique, 59655 Villeneuve d'Ascq Cedex, France*
[c] *Lehrstuhl für Angewandte Mathematik und Numerische Analysis, Fachbereich C – Mathematik und Naturwissenschaften, Bergische Universität Wuppertal, Gaußstr. 20, 42119 Wuppertal, Germany*

Abstract

Using pseudodifferential calculus and factorization theorems we construct a hierarchy of novel absorbing boundary conditions for the stationary Schrödinger equation with general (linear and nonlinear) potential. Doing so, we generalize the well-known quantum transmitting boundary condition of Kirk and Lentner to the case of space-dependent potential. Moreover, we propose a rapidly converging iterative method based on finite elements suitable for computing scattering solutions and bound states. The accuracy of our new absorbing boundary conditions is investigated numerically for two different situations. The first problem is related to the computation of linear scattering problems. The second application concerns the computation of energies and

*Corresponding author.
Email addresses: Xavier.Antoine@iecn.u-nancy.fr (Xavier Antoine), Christophe.Besse@math.univ-lille1.fr (Christophe Besse), ehrhardt@math.uni-wuppertal.de (Matthias Ehrhardt), Pauline.Klein@iecn.u-nancy.fr (Pauline Klein)
URL: http://www.iecn.u-nancy.fr/~antoine/ (Xavier Antoine), http://math.univ-lille1.fr/~besse/ (Christophe Besse), http://www-num.math.uni-wuppertal.de/~ehrhardt/ (Matthias Ehrhardt)

[1] Supported partially by the French ANR fundings under the project MicroWave NT09_460489 (http://microwave.math.cnrs.fr/).

ground-states for linear and nonlinear Schrödinger equations. It turns out that these absorbing boundary conditions and their variants lead to a higher accuracy than the usual Dirichlet boundary condition. Finally, our approach also offers the possibility to construct ABCs for higher dimensional problems.

Keywords: Absorbing boundary conditions, stationary Schrödinger equations, unbounded domain, spatially dependent potential
PACS: 03.65.-w, 42.82.Et, 43.30.Ma
2000 MSC: 35J10, 65M60, 65N30

---

1. Introduction

The solution of the Schrödinger equation occurs in many applications in physics, chemistry and engineering (e.g. quantum transport, condensed matter physics, quantum chemistry, optics, underwater acoustics, ...). The considered problem can appear in different forms: time-dependent or stationary equation, linear or nonlinear equation, inclusion of a variable potential among others. One of the main difficulty when solving the Schrödinger equation, and most particularly from a numerical point of view, is to impose suitable and physically admissible *boundary conditions* to solve numerically a bounded domain equation modeling an equation originally posed on an unbounded domain. Concerning the time-domain problem, many efforts have been achieved these last years. We refer the interested reader e.g. to the recent review paper [1] and the references therein for further details.

In this paper, we focus on the solution to the *stationary Schrödinger equation*. For a given potential V, eventually nonlinear ($V := V(x, \varphi)$, we want to solve the following equation

$$\left(-\alpha \frac{d^2}{dx^2} + V\right) \varphi = E\varphi, \qquad x \in \mathbb{R}, \tag{1}$$

or rewritten as

$$\left(\frac{d^2}{dx^2} + \frac{1}{\alpha}\big[E - V\big]\right) \varphi = 0, \qquad x \in \mathbb{R}, \tag{2}$$

with some parameter α that allows for some flexibility. More precisely, we study the extension of the recently derived *time-domain boundary conditions* [2] to the following two situations:

- **linear and nonlinear scattering:** E is a given value and the potential V being linear (independent of φ) or nonlinear, we want to compute φ as the solution of (1).

- **stationary states:** we determine here the pair (φ, E), for a given linear or nonlinear potential V. This eigenvalue problem is also known as the *computation of ground states*. The energy of the system is then the eigenvalue E and the associated stationary state is the eigenfunction φ. In particular, we seek the fundamental stationary state which is linked to the *smallest eigenvalue*. In practice, higher order states are also of interest.

For the stationary Schrödinger equation (2), boundary conditions for solving linear scattering problems with a constant potential outside a finite domain have been proposed e.g. by Ben Abdallah, Degond and Markowich [3], by Arnold [4] for a fully discrete Schrödinger equation and in a two-dimensional quantum waveguide by Lent and Kirkner [5, 6]. The case of bound states can be found for specific one-dimensional linear Schrödinger equations in [7, 8, 9, 10, 11]. These boundary conditions are needed e.g. to improve existing simulation tools for semiconductors that allows to investigate certain stationary (and also transient) behavior of the devices, like conductance, capacity, current-voltage curves. Often the physical relevant effects take place only in a small subregion of the device, and the novel absorbing boundary conditions offer the possibility to confine the computations to this small domain. We refer the reader to [12, 13, 14, 15] for more application details.

The goal of this work is to propose and validate some new boundary conditions for modeling linear and nonlinear variable potentials stationary one-dimensional Schrödinger equations with application to scattering and ground-state computation. We provide the whole theory which is related to previous developments [2] as well as numerical schemes for their validation. Finally, let us point out that these absorbing boundary conditions can be extended to higher dimensional problems and other situations like variable mass problems [16, 17, 18].

The paper is organized as follows. In Section 2, we explain how to obtain the stationary boundary conditions from the time-dependent case. Then, in Section 3, we investigate numerically these absorbing boundary conditions in the case of linear scattering problems. Section 4 and 5 are respectively devoted to their applications to linear and nonlinear eigenstate computation

with applications to many possible given variable potentials and nonlinearities. Finally, Section 6 draws a conclusion and give an outlook for possible future research directions.

2. Absorbing boundary conditions: from the time-domain to the stationary case

In order to derive some *absorbing boundary conditions (ABCs)* for the stationary Schrödinger equation (2), let us first start with the time-domain situation. In case of the *time-dependent Schrödinger equation* with a linear or nonlinear potential $\widetilde{V}$

$$\begin{cases} i\partial_t u + \partial_x^2 u + \widetilde{V} u = 0, & \forall (x,t) \in \mathbb{R} \times \mathbb{R}^+, \\ u(x,0) = u_0(x), & x \in \mathbb{R}, \end{cases} \tag{3}$$

the following *second- and fourth-order ABCs* on the boundary $\Sigma \times \mathbb{R}^+$

$$\text{ABC}_2^2\text{:} \qquad \partial_{\mathbf{n}} u = i \,\text{Op}\left(\sqrt{-\tau + \widetilde{V}}\right) u, \tag{4}$$

$$\text{ABC}_2^4\text{:} \qquad \partial_{\mathbf{n}} u = i \,\text{Op}\left(\sqrt{-\tau + \widetilde{V}}\right) u - \frac{1}{4}\,\text{Op}\left(\frac{\partial_{\mathbf{n}} \widetilde{V}}{-\tau + \widetilde{V}}\right) u, \tag{5}$$

were derived recently in [2]. Here, Op denotes a pseudodifferential operator and the fictitious boundary Σ is located at the two interval endpoints x_ℓ and x_r. The outwardly directed unit normal vector to the bounded computational domain $\Omega =]x_\ell; x_r[$ is denoted by $\mathbf{n}$.

To obtain some ABCs for the stationary equations (1) or (2), we consider these equations supplied with a new potential: $\widetilde{V} := -V/\alpha$. Moreover, we are seeking some *time-harmonic solutions* $u(x,t) := \varphi(x) e^{-i\frac{E}{\alpha}t}$ and since

$$i\partial_t u = \frac{E}{\alpha} \varphi(x)\, e^{-i\frac{E}{\alpha}t},$$

the variable $-\tau$ can be identified with E/α. These considerations yield some *stationary ABCs* that we designate by SABC^M ('S' stands for stationary and M denotes the order of the boundary condition) :

$$\text{SABC}^2\text{:} \qquad \partial_{\mathbf{n}} \varphi = i \frac{1}{\sqrt{\alpha}} \sqrt{E - V}\, \varphi, \quad \text{on } \Sigma, \tag{6}$$

$$\text{SABC}^4\text{:} \qquad \partial_{\mathbf{n}} \varphi = i \frac{1}{\sqrt{\alpha}} \sqrt{E - V}\, \varphi + \frac{1}{4} \frac{\partial_{\mathbf{n}} V}{E - V}\, \varphi, \quad \text{on } \Sigma. \tag{7}$$

The second- and fourth-order ABCs for the time-dependent Schrödinger equation (4), (5) were developed under a *high frequency assumption* $\tau \gg 1$ [2]. This relation can be translated to the stationary case in terms of links between E and V. The new relations will be given for the different scattering or eigenvalues problems in the next dedicated sections.

Remark 1. For the time-dependent case [2], we constructed two families of ABCs, denoted by ABC_1^M and ABC_2^M. These ABCs all coincide if the potential is time-independent. In the stationary case, all the potentials fall into this category and thus the ABCs are equivalent. Hence, we get the unique class of stationary ABCs, SABC^M (without subscript index). For convenience, the form of the boundary conditions (6)–(7) is based on ABC_2^M (we refer to [2] for more technical details).

3. Application to linear scattering problems

3.1. Problem formulation and finite element approximation

Let us consider an incident right-traveling plane wave

$$\varphi^{\mathrm{inc}}(x) = e^{ikx}, \quad k > 0, \qquad x \in]-\infty; x_\ell], \tag{8}$$

coming from $-\infty$. The parameter k is the real valued positive wave number and the variable potential V in (1) models an inhomogeneous medium. We consider a bounded computational domain $\Omega =]x_\ell; x_r[$ and assume that the scattered wave $\varphi - \varphi^{\mathrm{inc}}$ is perfectly reflected back at the left endpoint x_ℓ. Furthermore, we assume that the total wave is transmitted in $[x_r; \infty[$, propagating then towards $+\infty$. As a consequence, we have to solve the following *boundary value problem*

$$\begin{aligned} &\left(-\alpha\frac{d^2}{dx^2} + V\right)\varphi = E\varphi, && \text{for } x \in \Omega, \\ &\partial_{\mathbf{n}}\varphi = g_{M,\ell}\varphi + f_{M,\ell}, && \text{at } x = x_\ell, \\ &\partial_{\mathbf{n}}\varphi = g_{M,r}\varphi, && \text{at } x = x_r, \end{aligned} \tag{9}$$

with $f_{M,\ell} = \partial_{\mathbf{n}}\varphi^{\mathrm{inc}}(x_\ell) - g_{M,\ell}\varphi^{\mathrm{inc}}(x_\ell)$. Here, the order M is equal to 2 or 4 according to the choice of SABC^M (6) or (7) and thus we have

$$g_{2,(\ell,r)} := i\frac{1}{\sqrt{\alpha}}\sqrt{E - V_{\ell,r}}, \tag{10}$$

$$g_{4,(\ell,r)} := g_{2,(\ell,r)} + \frac{1}{4}\frac{\partial_{\mathbf{n}}V_{|x=x_{\ell,r}}}{E - V_{|x=x_{\ell,r}}}. \tag{11}$$

In the sequel of this paper, we will also use the following other concise writing

$$\partial_{\mathbf{n}}\varphi = g_M\varphi + f_M, \quad \text{on } \Sigma, \tag{12}$$

for each function being adapted with respect to the endpoint. Finally, for a plane wave, we have the *dispersion relation*: $E = \alpha k^2 + V_\ell$, where $V_\ell = V(x_\ell)$.

In the sequel all the potentials are supposed to be smooth, at least in the two unbounded exterior domains $]-\infty; x_\ell]$ and $[x_r; \infty[$, which is compatible with the theory of pseudodifferential operators [19]. Furthermore, to compute a numerical reference solution, we assume that the potentials are either constant outside a large reference domain or numerically zero outside this domain.

We use a *finite element method (FEM)* to solve numerically this problem. One benefit of using FEM in this application is that the ABCs can be incorporated directly into the variational formulation. The interval $[x_\ell; x_r]$ is decomposed into n_h elementary uniform segments of size h. Classically, the ABCs are considered as *(impedance) Fourier-Robin boundary conditions*. Let $\boldsymbol{\varphi} \in \mathbb{C}^{n_h+1}$ denote the vector of nodal values of the $\mathbb{P}_1$ interpolation of φ and let $\mathbb{S} \in \mathcal{M}_{n_h+1}(\mathbb{R})$ the $\mathbb{P}_1$ stiffness matrix associated with the bilinear form

$$\int_\Omega \partial_x\varphi\, \partial_x\psi\, dx.$$

Next we introduce $\mathbb{M}_{V-E} \in \mathcal{M}_{n_h+1}(\mathbb{R})$ as the *generalized mass matrix* arising from the linear approximation of

$$\int_\Omega (V - E)\varphi\psi\, dx,$$

for any test-function $\psi \in H^1(\Omega)$. Let $\mathbb{B}_M \in \mathcal{M}_{n_h+1}(\mathbb{C})$ be the matrix of the boundary terms related to the ABC SABC^M

$$\mathbb{B}_M = \begin{pmatrix} \alpha g_{M,\ell} & 0 & 0 & 0 \\ 0 & \dots & \dots & 0 \\ 0 & \dots & \dots & 0 \\ 0 & \dots & \dots & 0 \\ 0 & 0 & 0 & \alpha g_{M,r} \end{pmatrix}. \tag{13}$$

The right-hand side vector $\mathbf{b}_M \in \mathbb{C}^{n_h+1}$ is given by

$$\mathbf{b} = \begin{pmatrix} \alpha f_{M,\ell} \\ 0 \\ \vdots \\ 0 \end{pmatrix}. \tag{14}$$

Finally, the linear system reads

$$(\alpha\mathbb{S} + \mathbb{M}_{V-E} + \mathbb{B}_M)\boldsymbol{\varphi} = \mathbf{b}_M, \tag{15}$$

which is solved by a LU method.

3.2. Numerical results

3.2.1. The case of a Gaussian potential

We study the stationary Schrödinger equation (1) with $\alpha = 1/2$:

$$-\frac{1}{2}\frac{d^2}{dx^2}\varphi + V\varphi = E\varphi, \quad x \in \mathbb{R}, \tag{16}$$

and consider an incident right-traveling plane wave with wave number $k = 10$. We first analyze the numerical results for a *Gaussian potential*

$$V(x) = A\, e^{-\frac{(x-x_c)^2}{w^2}}, \tag{17}$$

centered at $x_c = 20$ with the amplitude $A = -5$ and the parameter $w = 3$ (see Figure 1). The choice of these parameters insures that $V(0)$ is sufficiently small such that the classical transparent boundary condition [3, 4] can be applied to the left boundary.

The numerical reference solution is computed on the large domain $]0; 60[$ using the fourth-order ABC. At the fictitious boundary points x_ℓ and x_r of the computational domain, the values of the potential are $V(60) \approx 10^{-77}$ and $V(0) \approx 10^{-19}$, i.e. from a numerical point of view, the potential can be considered as compactly supported in this reference domain. Then, the ABCs are highly accurate [1] yielding a suitable *reference solution* φ_{ref} with spatial step size $h = 5 \cdot 10^{-3}$. Let us remark here that the case of non-compactly supported initial data was treated in [20].

We next compute the solution obtained by applying the ABCs on a smaller computational domain by shifting the right endpoint to $x_r = 18$,

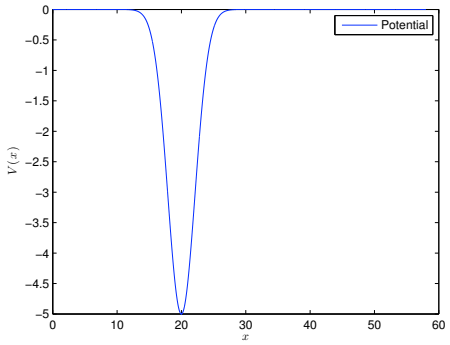

Figure 1: Gaussian potential $V(x) = -5e^{-(x-20)^2/9}$.

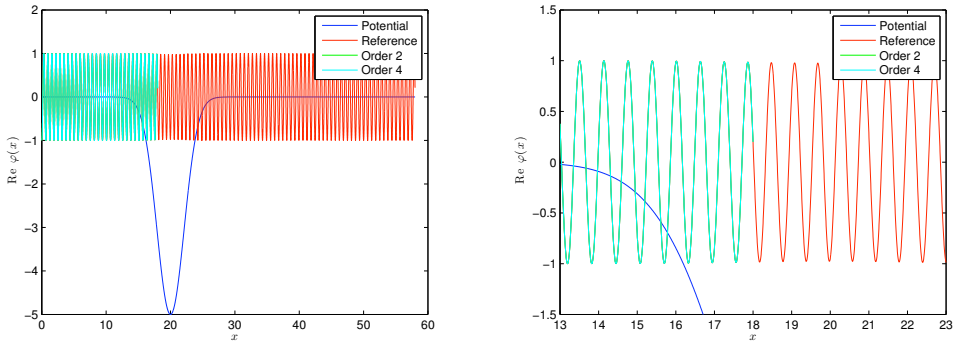

(a) Real part

(b) Zoom at $x_r = 18$

Figure 2: Real parts of the numerical solutions.

now the potential being far from vanishing at this endpoint. In the negative half-space $x < x_\ell = 0$, the potential is almost equal to zero and hence the second-order ABC is very accurate. Note that this latter condition will be always used at the left endpoint and we only analyze the effect of the ABC on the right fictitious endpoint x_r. We keep the step size $h = 5 \cdot 10^{-3}$ as for the reference solution. Figure 2 shows the computed solutions (denoted by φ_{num}), superposed on the potential and reference solution, with the second-order (green) and fourth-order (cyan) ABCs placed at the right endpoint x_r. Since the solutions are complex valued, we only plot here their real parts. Note that we would obtain roughly the same curves for their complex parts. The ABCs give quite good results as it can be clearly observed in Figure 2(b)

where we zoom around the boundary $x_r = 18$ to distinguish the different curves. At first sight, the curves coincide. Next we plot in Figure 3(a) the error curves on the real part $x \mapsto |\operatorname{Re}(\Delta\varphi(x))|$ and in Figure 3(b) we show the modulus $x \mapsto |\Delta\varphi(x)|$, with the error $\Delta\varphi = \varphi_{\text{num}} - \varphi_{\text{ref}}$. We can see that

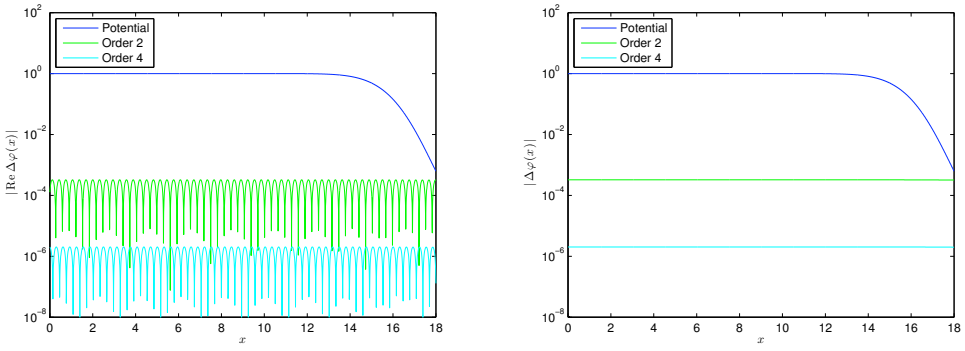

(a) Error on the real part

(b) Error on modulus

Figure 3: Errors $|\varphi_{\text{num}} - \varphi_{\text{ref}}|$ for the potential $V(x) = -5e^{-(x-20)^2/9}$.

the approximation error by using the SABC^2 is roughly $5 \cdot 10^{-4}$ while the error associated with ABC^4 is almost 10^{-6}, which is also the linear finite element approximation error $h^2 \approx 10^{-6}$. Hence, not only the results are precise but they are also of increasing accuracy as the order of the SABC increases.

The amplitude and phase of the solution are modified depending on the chosen potential. To analyze this point, we consider an incident plane wave $\varphi^{\text{inc}}(x) = e^{ikx}$ with the wave number $k = 8$ and the potential

$$V(x) = A\, e^{-\frac{(x-20)^2}{9}},$$

where the amplitude A will vary. The Figure 4 shows the potential as well as the reference solution, where the potential amplitude is set to $A = -50$. In Figure 4(a) we observe on the real part an attenuation of the wave amplitude in the zone where the potential is numerically not zero. We also notice stronger oscillations in this zone, see Figure 4(b). Figure 5 shows some analogous results for $A = 20$. For this case we observe in Figure 5(a) that the amplitude of the wave increases and that its frequency decreases, see Figure 5(b).

We next study the evolution of the error related to the wave number k. Since the ABCs are developed under a *high frequency assumption* [2],

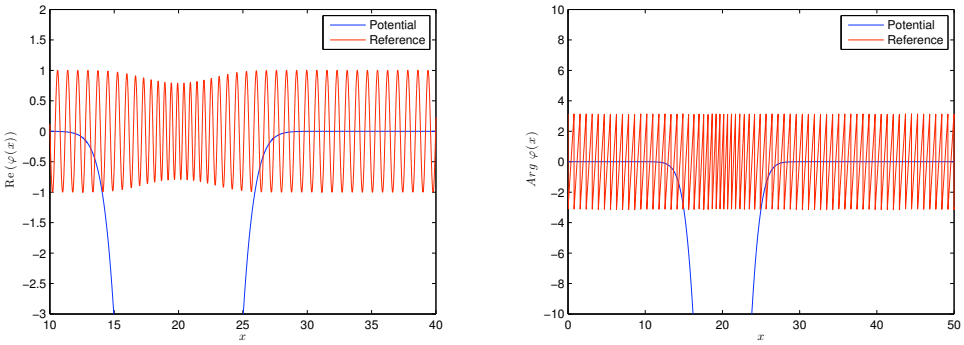

(a) Real part (b) Argument

Figure 4: Modification of the frequency of the wave field when passing through the potential according to the amplitude of V ($V(x) = -50\, e^{-(x-20)^2/9}$ and wave number $k = 8$).

we should observe a gain of accuracy for large values of k. To check it, we compute the maximum of the error in the computational domain $[0; x_r]$ as a function of the wave number k. Indeed, we clearly recognize that the error curves have always the same behaviour, they are periodic with an error peak corresponding to the extrema of the solution. Therefore, the error is suitably described by $\max_{x\in[0;x_r]} |\Delta\varphi(x)|$. We report in Figure 6 the results for the ABCs of orders two and four depending on k.

In Figure 6(a) we first observe that the error decays for increasing wave number k and that SABC^4 is more accurate than SABC^2 for a wave amplitude $A = 1$. We also remark a loss of accuracy of the ABCs when k grows (about $k = 8$). The two ABCs lead to the same accuracy which is not *a priori* compatible with the high frequency assumption. However, the deterioration is not due to the ABCs but to the finite element method which suffers from the so-called *pollution error* for high wave numbers [21]. To confirm this hypothesis, we refine the mesh size by a factor 10: $h = 5 \cdot 10^{-4}$, and report the results in Figure 6(b) showing that the ABCs give a precision increasing with their respective order between $k = 8$ and $k = 20$. Figure 7 shows the same results as Figure 6 but for a potential amplitude equal to $A = -5$ (instead of $A = 1$), the conclusion being the same.

Let us now answer the question: *Where can we place the fictitious boundary for a given problem?* To this end, we perform a couple of experiments for the Gaussian potential (17) centered at $x_c = 20$ with $w = 3$ and a varying amplitude A. For a fixed value of k, we let x_r vary. We observe that the

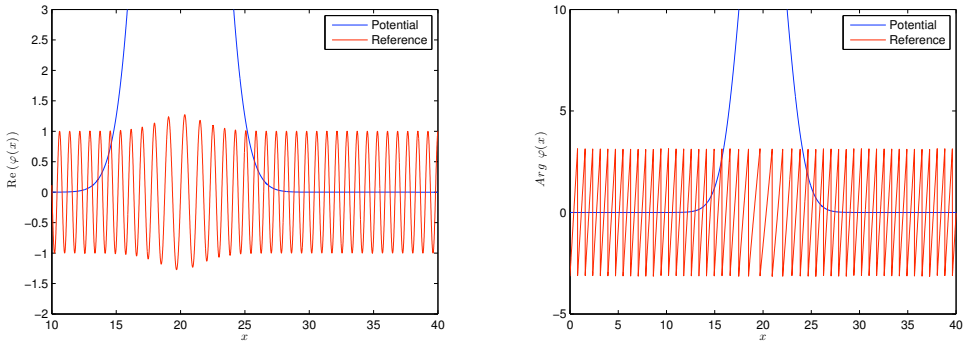

(a) Real part (b) Argument

Figure 5: Modification of the frequency of the wave field when passing through the potential according to the amplitude of V ($V(x) = 20\, e^{-(x-20)^2/9}$ and $k = 8$).

error depends on the amplitude of the potential A (see for example Fig. 11). If A is negative, then x_r can be placed both at the right or left of the center of the Gaussian x_c. When the amplitude A is positive, we observe the same kind of situation but only if A is not too large otherwise the results are completely incorrect if $x_r \leq x_c$ and become accurate when x_r is larger than x_c. A similar conclusion can be made if x_r is chosen to be smaller than x_c but for a variable wave number k. We observe in Figures 8(a), 9(a) and 9(b) that there exists limit values of the amplitude A (respectively 50, 32 and 72) that lead to a bad behavior of the ABCs. Hence, we conjecture that there exists a critical value of A which is related to k, x_r and x_c. Let us fix the wave number $k = 10$ and the right fictitious boundary $x_r = 18$ (cf. Figure 10), i.e. we are in the situation $x_r < x_c$ since $x_c = 20$. To explain these remarks, let us recall that the dispersion relation connecting the energy $E = E(k)$ to the wave number k is

$$E = \frac{k^2}{2} + V_\ell. \tag{18}$$

We replace E in equation (16) by the above expression to obtain

$$-\frac{1}{2}\varphi'' + V\varphi = \frac{k^2}{2}\varphi + V_\ell\varphi,$$

i.e.

$$\varphi'' + \left[k^2 - 2(V - V_\ell)\right]\varphi = 0.$$

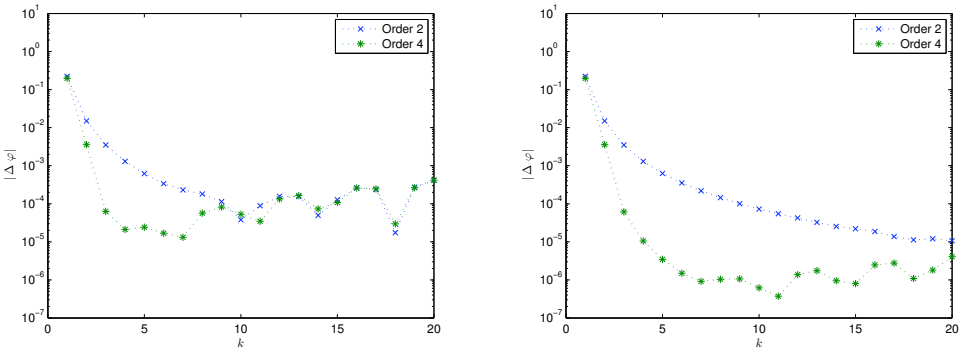

(a) $h = 5 \cdot 10^{-3}$ (b) $h = 5 \cdot 10^{-4}$

Figure 6: Evolution of the error as a function of k and for two spatial steps ($A = 1$).

For the Gaussian potential case with suitable chosen parameters x_c and w, $V_\ell = V(0)$ is numerically almost zero (for $A = 1$, $x_c = 20$ and $w = 3$), the value of the potential is 10^{-20} at $x_\ell = 0$), thus we have to solve numerically the equation

$$\varphi'' + \left(k^2 - 2V\right)\varphi = 0. \tag{19}$$

The properties of the solution to (19) strongly depend on the sign of $k^2 - 2V$. This term can be regarded as a new (variable) wave number $\tilde{k}^2$ which must be positive on $[x_r; +\infty[$ to obtain an accurate ABC, i.e. the minimum of this term must be positive, which yields the condition

$$\max_{x \in [x_r; +\infty[} V(x) \leq \frac{k^2}{2}. \tag{20}$$

This relation (20) involves three parameters: k, A and x_r. For a given wave number k, fixing A imposes that x_r is large enough and on the other hand, fixing x_r requires that A is not too large. More precisely, the maximum of V on $[x_r; +\infty[$ is

$$\begin{cases} \max\limits_{x \in [x_r; +\infty[} V(x) = V(x_c) = A, & \text{if } x_r < x_c, \\ \max\limits_{x \in [x_r; +\infty[} V(x) = V(x_r), & \text{if } x_r \geq x_c. \end{cases} \tag{21}$$

We then have two cases. In the first case, k and A satisfy the relation

$$A \leq \frac{k^2}{2}. \tag{22}$$

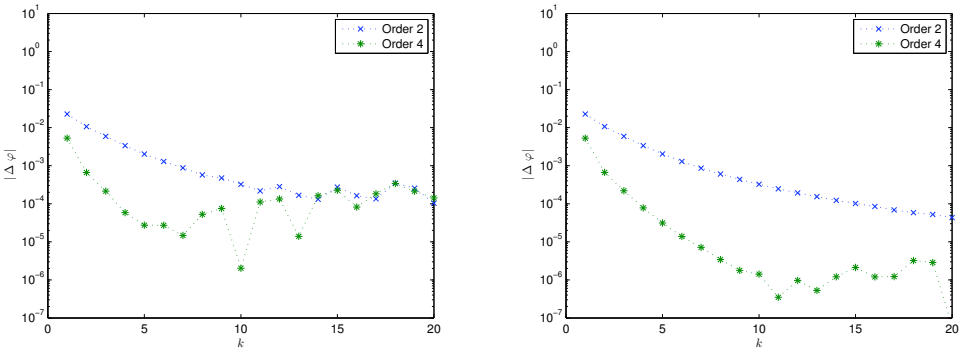

(a) $h = 5 \cdot 10^{-3}$ (b) $h = 5 \cdot 10^{-4}$

Figure 7: Evolution of the error according to k and for two spatial steps ($A = -5$).

Hence, whatever the value of x_r is, the relation (20) is always fulfilled and x_r can be placed freely according to x_c. In the second situation, relation (22) is not always fulfilled. Indeed, the three parameters must verify

$$A \exp\left(-\frac{(x_r - x_c)^2}{w^2}\right) \leq \frac{k^2}{2}, \tag{23}$$

which lead to choose x_r larger than x_c. More precisely, an approximate minimal value $x_r^{\min}$ of x_r is

$$x_r^{\min} \approx x_c + w\sqrt{\ln\left(\frac{2A}{k^2}\right)}. \tag{24}$$

Remark 2. The condition ensuring that $\tilde{k}^2 = k^2 - 2(V - V_\ell)$ remains positive on $[x_r; +\infty[$ is the same as having well-defined ABCs. Indeed, writing $k^2 = 2(E - V_\ell)$, we get

$$\begin{aligned} k^2 - 2(V - V_\ell) \geq 0 \quad &\Leftrightarrow \quad 2(E - V_\ell) - 2(V - V_\ell) \geq 0 \\ &\Leftrightarrow \quad E - V \geq 0. \end{aligned}$$

Then, in the second- and fourth-order ABCs, (6) and (7), we have $E - V_r \geq 0$ and $\sqrt{E - V_r}$ is well-defined.

In the example of the Gaussian potential and for $k = 10$, the critical amplitude from (22) to have no constraint on x_r is $A = 50$. To prove this

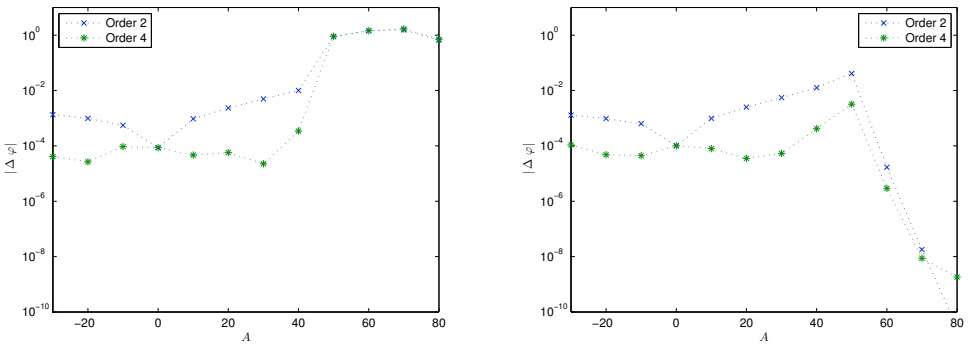

(a) $x_r = 18$ (b) $x_r = 22$

Figure 8: Evolution of the error with respect to the amplitude A ($k = 10$).

numerically, we compute the error $|\Delta\varphi|$ associated with each boundary condition as a function of A for some values in $]-30; 80[$. In Figure 8(a), for $x_r = 18$ and $x_c = 20$, we remark that the results are accurate and the accuracy of the ABCs is related to their order M, until $A = 40$. When approaching the critical value $A = 50$, the error grows and then yields wrong results. We perform a similar test in Figure 8(b) but fixing now $x_r = 22$, (cf. Figure 10). We now observe that we do not have any restriction on the amplitude and that the results are always accurate.

In the series of curves in Figure 11, we present the error $|\Delta\varphi|$ for a potential centered at $x_c = 20$ with a given amplitude A (-20, 30, 50, 60) and $k = 10$ depending on the location of the right endpoint x_r. For the two first Figures 11(a) and (b) ($A = -20$ and $A = 30$), we are in a configuration where $2A < k^2$. We observe a high accuracy of our results which is due to the fact that there is no *a priori* restriction on the location x_r. Figure 11(c) concerns the limit case when $2A = k^2$. According to (24), the results are correct for $x_r \geq x_r^{\min} = 20$. Finally, the last figure corresponds to $2A > k^2$ and is globally coherent with the condition (24). Choosing $x_r < x_c$ does not yield accurate results which was predictable according to the previous analysis. A little bit more surprising is that the results become more accurate when $x_r > x_c$ even if the theoretical value for $A = 60$ is $x_r^{\min} \approx 21.3$. However, we clearly observe a great accuracy improvement after $x_r = 21$. In particular, we remark the difference in the accuracy between the ABCs of order two and four after this value, the fourth-order ABC being the most accurate one.

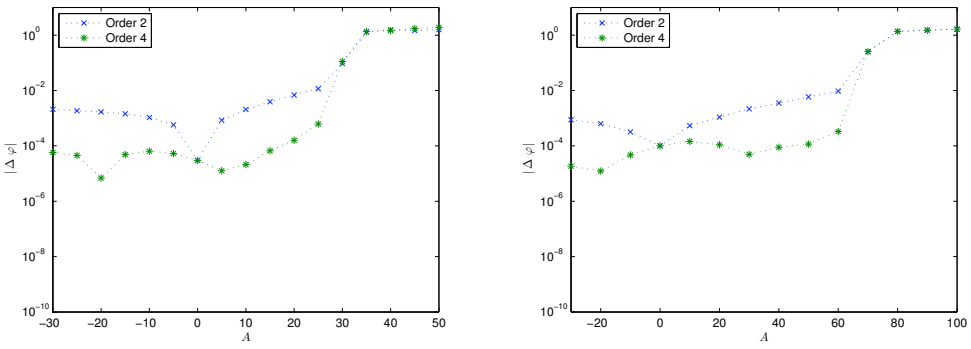

(a) $x_r = 18$, $k = 8$ (b) $x_r = 18$, $k = 12$

Figure 9: Evolution of the error with respect to the amplitude A for various values of k.

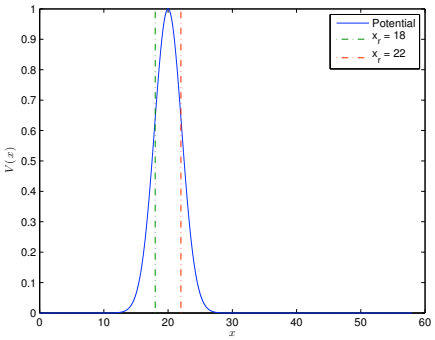

Figure 10: Gaussian potential and placement of the fictitious boundary ($A = 1$).

3.2.2. The case of a double Gaussian potential

To complete the previous study, we analyze now the case where the potential is the sum of two Gaussian potentials in the reference domain $]0; 50[$

$$V(x) = A_1 \exp\left(-\frac{(x - x_{c_1})^2}{w_1^2}\right) + A_2 \exp\left(-\frac{(x - x_{c_2})^2}{w_2^2}\right). \tag{25}$$

To start with we fix the parameters

$$x_{c_1} = 24, \quad x_{c_2} = 34, \quad w_1 = 5, \quad w_2 = 4, \tag{26}$$

and let the amplitudes A_1 and A_2 vary. In the whole section we use the wave number $k = 10$ and the step size $h = 5 \cdot 10^{-3}$.

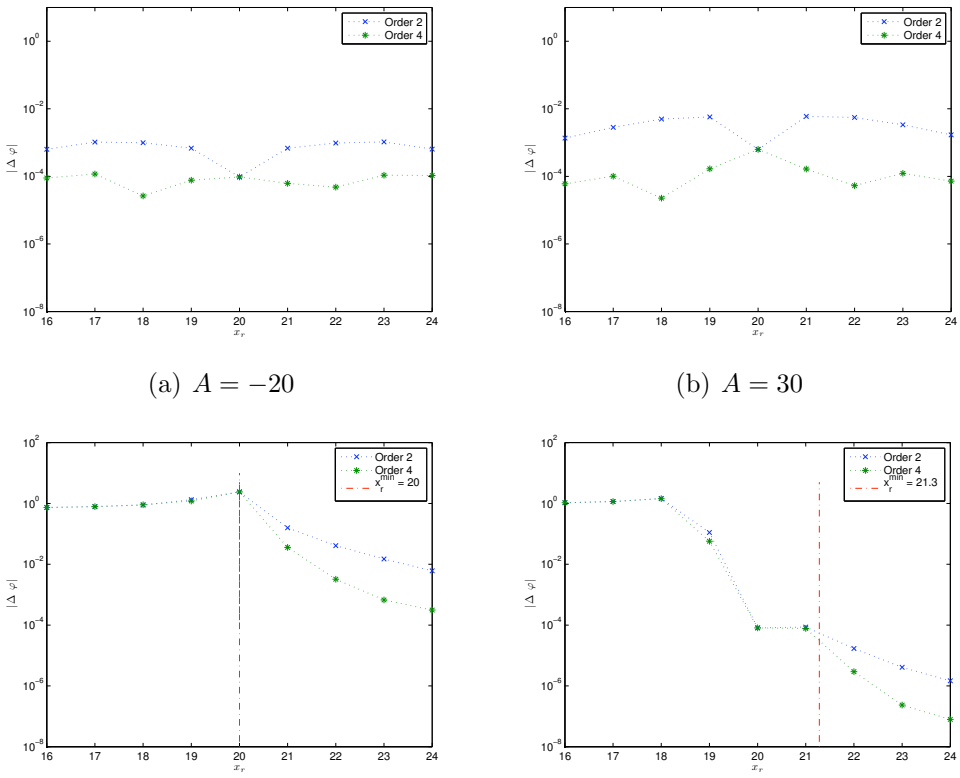

(a) $A = -20$ (b) $A = 30$

(c) $A = 50$ (d) $A = 60$

Figure 11: Evolution of the error according to x_r (A is fixed, $k = 10$ and $x_c = 20$).

Figure 12 presents the results for this potential. We place the right endpoint $x_r = 26$ and plot the resulting error on the real part in Figure 12(b). The ABCs perform well even if the fictitious boundary is in the middle of the potential. Again, we observe the hierarchy between the ABCs.

Figure 13 proposes another situation for the double Gaussian potential with a step between the two Gaussians and $x_r = 15$ located in this gap. In this example, the solutions computed with the ABCs are very accurate with an error (in infinite norm) less than 10^{-4}. The errors for both ABCs are the same here since x_r is placed between the two Gaussians, where the potential is flat. As a consequence, its derivative is almost equal to zero at this point: $\partial_x V(15) \approx 10^{-3}$, leading numerically to the same precision of both boundary conditions.

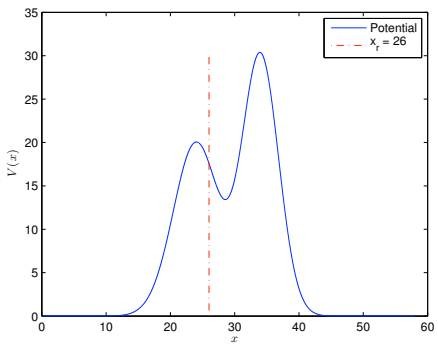

(a) Potential and fictitious boundary

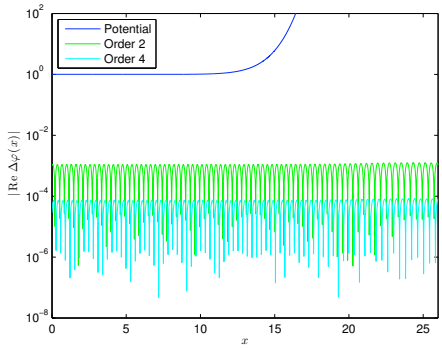

(b) Error on the real part

Figure 12: Double Gaussian potential: $V(x) = 20\, e^{-\frac{(x-24)^2}{25}} + 30e^{-\frac{(x-34)^2}{16}}$.

3.2.3. Other potentials: partially quadratic, double barrier with quadratic part

The first potential is a quadratic potential defined on $[0; 20]$ by

$$V(x) = \begin{cases} 2 + (x-8)^2, & \text{for } x \in [0; 8], \\ 2, & \text{for } x \in]8; 20]. \end{cases} \tag{27}$$

Figure 14 shows the results for $x_r = 3$ and step size $h = 5 \cdot 10^{-3}$. Since the potential is constant outside $[0; 8]$, we can compute a reference solution by applying an exact ABC, a so-called *transparent boundary condition (TBC)* [1] on x_ℓ and x_r. The second-order ABC gives an error of about $5 \cdot 10^{-3}$ and the fourth-order ABC an error equal to 10^{-4}.

The last potential, illustrated in Figure 15, is a double barrier potential with a quadratic part given by the analytic expression

$$V(x) = \begin{cases} 35/2, & x \leq 15 \\ 25 - x/2, & 15 \leq x \leq 20 \text{ et } 23 \leq x \leq 26 \\ 29 - x/2, & 20 \leq x \leq 23 \text{ et } 26 \leq x \leq 29 \\ 21/2 + \left((x-38)^2 - (29-38)^2\right)/20, & 29 \leq x \leq 38 \\ 21/2 - (29-38)^2/20, & x \geq 38. \end{cases} \tag{28}$$

Here, the basic difference to the potential (25) is the presence of discontinuities in the computational domain. As a consequence, the fictitious point

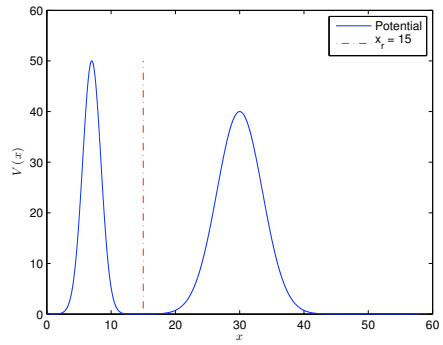

(a) Potential

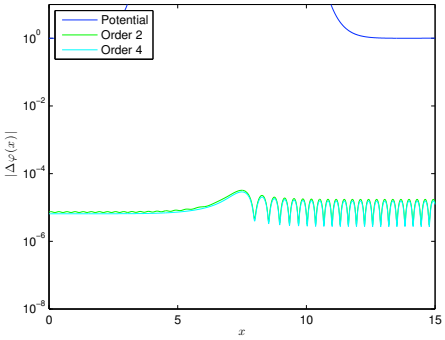

(b) Error on modulus

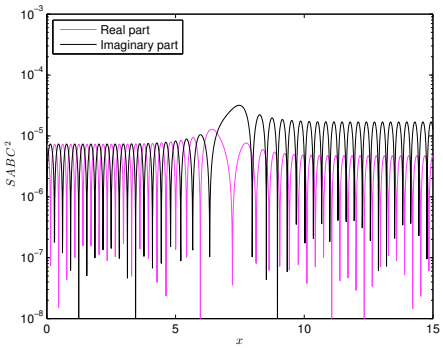

(c) SABC^2

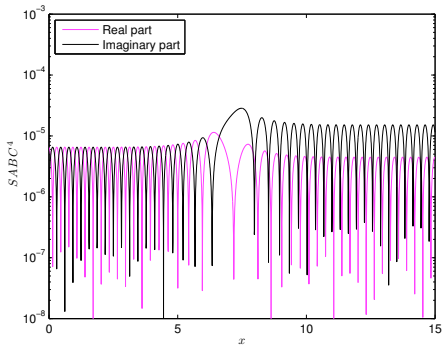

(d) SABC^4

Figure 13: Double Gaussian potential: $V(x) = 50\,e^{-\frac{(x-7)^2}{4}} + 40\,e^{-\frac{(x-30)^2}{25}}$. The bottom figures present the error on the real and imaginary parts for each ABC.

x_r cannot be placed between the two barriers (at $x_r = 24$ or $x_r = 27$ for example). So, we have to choose the right end point x_r between 29 and 38 (after 38, the potential is constant and the ABCs are exact). We decide to fix here $x_r = 31$ in this example. As we can see, the error with SABC^4 is slightly better than with SABC^2 which is already less than 10^{-4}.

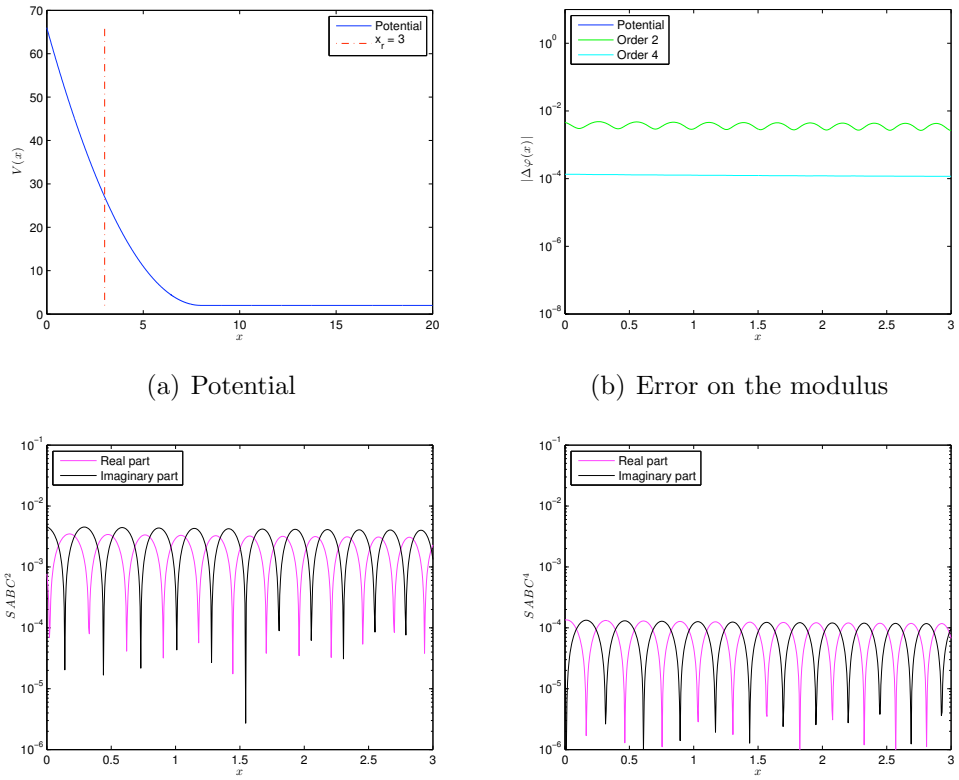

(a) Potential

(b) Error on the modulus

(c) SABC^2

(d) SABC^4

Figure 14: Quadratic potential ($x_r = 3$). The bottom figures present the error in the real and imaginary parts for each condition.

4. Application to the computation of stationary states: the linear case

The second problem for testing the ABCs is the following. Let us consider the Hamiltonian H

$$H = -\alpha \frac{d^2}{dx^2} + V(x), \qquad x \in \mathbb{R}, \tag{29}$$

defined through α and V. The task here is to determine the pair (ϕ_E, E) solution to the *eigenvalue problem*

$$H\phi_E = E\phi_E, \qquad x \in \mathbb{R}. \tag{30}$$

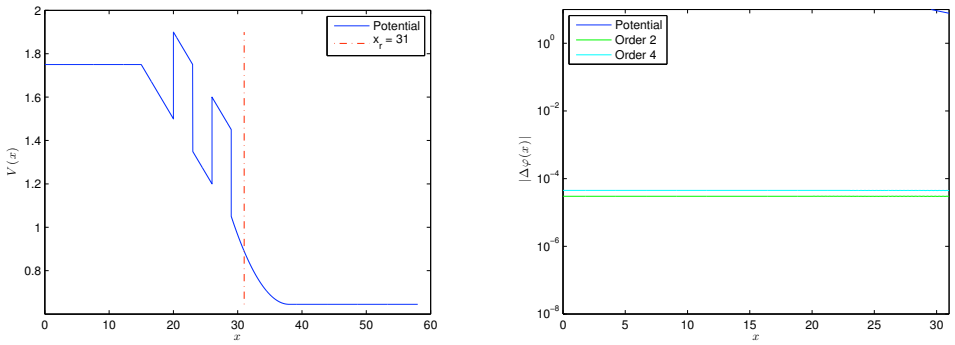

(a) Potential (b) Error on modulus

Figure 15: Double barrier potential with quadratic part ($x_r = 31$).

This problem can also be formulated as follows: find the eigenvalues $(E_n)_{n\in\mathbb{N}}$ (energies) and the associated real-valued eigenfunctions $(\phi_n)_{n\in\mathbb{N}}$ (eigenstates or ground states) as solutions of

$$H\phi_n = E_n\phi_n, \qquad x \in \mathbb{R}. \tag{31}$$

To fix the eigenfunction, it is necessary to impose a *normalization condition*

$$\|\phi\|_{L^2(\mathbb{R})} = 1, \tag{32}$$

or

$$\|\phi_E\|_{L^2(\mathbb{R})} = 1. \tag{33}$$

Let us begin with the case where the potential does not depend on the eigenfunction (called linear case here). The nonlinear case will be treated later in Section 5.

4.1. Square-root ABCs

Before discussing the difficulties related to the ABCs, let us consider the numerical solution of our problem with a homogeneous Dirichlet boundary condition. The variational formulation of (30) reads

$$-\alpha[\partial_{\mathbf{n}}\phi_E\psi]_{x_\ell}^{x_r} + \alpha\int_\Omega \partial_x\phi_E\partial_x\psi\,dx + \int_\Omega V\phi_E\psi\,dx = E\int_\Omega \phi_E\psi\,dx, \tag{34}$$

for some test-functions $\psi \in H_0^1(\Omega)$ [22]. Let $\mathbb{S}^0$, $\mathbb{M}^0$ and $\mathbb{M}_V^0$ be respectively the stiffness matrix, mass and generalized mass matrices associated with the

potential V for $\mathbb{P}_1$ finite element and a homogeneous Dirichlet boundary condition (these matrices are some elements of $\mathcal{M}_{n_h-1}(\mathbb{R})$). The discrete problem can be classically formulated as the following *generalized eigenvalue problem*: find the pair $(E, \boldsymbol{\phi}_E)$ as solution to

$$\begin{cases} \left(\alpha\mathbb{S}^0 + \mathbb{M}_V^0\right)\boldsymbol{\phi}_E = E\mathbb{M}^0\boldsymbol{\phi}_E, \\ \|\mathbb{M}^0\boldsymbol{\phi}_E\|_2 = 1, \end{cases} \tag{35}$$

which is a generalized eigenvalue problem with an equality constraint. Here, $\boldsymbol{\phi}_E$ is a vector in $\mathbb{R}^{n_h-1}$ which is normalized by: $\|\mathbb{M}^0\boldsymbol{\phi}_E\|_2 = 1$ ($\|\cdot\|_2$ being the usual Euclidian norm in $\mathbb{R}^{n_h-1}$). The global algorithm complexity is essentially the sum of the complexities for building the sparse finite element matrices and for computing the eigenvalue problem.

In this paper, we use Matlab's `eigs` function which provides the p smallest positive eigenvalues corresponding to the generalized eigenvalue problem. This function automatically normalizes the eigenvectors in the Euclidian norm hence fulfilling the normalization constraint in (35). `eigs` is associated with the software `ARPACK` (http://www.caam.rice.edu/software/ARPACK/).

In the case where the potential is not always positive, we use the property that the smallest eigenvalue E_0 is larger than the minimum of the potential $V_{\min}$ and solve (35) by a translation of $-V_{\min}$. Finally, the solution to (35) generates the sequence of the p first eigenvalues $(E_n^0)_{0\leq n\leq p-1}$, eigenvectors $(\boldsymbol{\phi}_n^0)_{0\leq n\leq p-1}$ and finite element eigenfunctions $(\phi_n^0)_{0\leq n\leq p-1}$ associated with the Dirichlet boundary condition. Since this eigenvalue problem is linear with respect to E, we can solve it without using e.g. a fixed point algorithm, unlike the case of including a square-root ABC as it is explained below. For this reason, the solution is called *"direct"* in the sequel of the paper.

Let us consider now the SABC^2 boundary condition

$$\partial_{\mathbf{n}}\phi_E = \frac{i}{\sqrt{\alpha}}\sqrt{E-V}\,\phi_E, \quad \text{on } \Sigma. \tag{36}$$

The main difficulty with this boundary condition is its nonlinear dependence on E. As a consequence, we cannot isolate the terms (E, ϕ_E) in the right-hand side of (34) in a linear way, that is under the form $E\phi_E$. More precisely, the *nonlinear eigenvalue problem* to solve is

$$\begin{cases} \left(\alpha\mathbb{S} + \mathbb{M}_V + \mathbb{B}_M(E^M)\right)\boldsymbol{\phi}^M = E^M\mathbb{M}\boldsymbol{\phi}^M, \\ \|\mathbb{M}\boldsymbol{\phi}^M\|_2 = 1, \end{cases} \tag{37}$$

using the matrix notations of the scattering problem. We precise that both the eigenvalues and eigenfunctions depend on the chosen boundary condition SABC^M by the notation: (E^M, ϕ^M). The first p eigencomponents are indexed as follows: (E_n^M, ϕ_n^M), with $0 \leq n \leq p-1$. The nonlinear dependence on the boundary term is given by the presence of $\mathbb{B}_M(E^M)$. To solve the eigenvalue problem with SABC^M, we have to apply an iterative scheme like a fixed point method (with a prescribed tolerance ϵ) and update E^M at each iteration step j.

This procedure implies that we have to *a priori* choose an eigenvalue of index n (denoted by E_n^M) that we wish to calculate. This is an important drawback since we have to *a priori* compute successively all the eigenvalues and associated eigenvectors. In fact, it appears that `eigs` is also able to provide an approximation of the first p eigenvalues $(E_n^{M,j})_{0\leq n\leq p-1}$ of $(E_n^M)_{0\leq n\leq p-1}$ and the corresponding eigenvectors $\boldsymbol{\phi}_n^M$. As a consequence, we also have to recompute the boundary terms arising in $\mathbb{B}_M(E_n^{M,j})$. Hence, the *fixed point algorithm* reads

$$\begin{cases} \left(\alpha\mathbb{S} + \mathbb{M}_V + \mathbb{B}_M(E_n^{M,j})\right)\boldsymbol{\phi}^{M,j+1} = E^{M,j+1}\mathbb{M}\boldsymbol{\phi}^{M,j+1}, \\ \|\mathbb{M}\boldsymbol{\phi}^{M,j+1}\|_2 = 1, \end{cases} \tag{38}$$

each linear problem being solved by using the Matlab routine `eigs`. More generally, for a boundary condition with a nonlinear dependence on the energy E, we use an associated fixed point algorithm. Even if we iterate through a fixed point algorithm, it appears that the algorithm also simultaneously gives some approximations of the other eigenvalues and eigenvectors (see the numerical section). This approach is therefore designated by *"direct"* if we only iterate on one *a priori* fixed eigenvalue. This algorithm can be applied successively by iteration using the fixed point algorithm and keeping only the computed eigenvalue and eigenvector related to the current iteration. Of course, the resulting algorithm is more expensive but at the same time more accurate. This approach is designated by *"loop"* in the sequel. Let us remark that there is no difference between both approaches for the Dirichlet problem.

4.2. Linearized ABCs

Unlike the case of the Dirichlet problem, we previously saw that the algorithm related to the square-root ABCs is iterative because of the nonlinearity. To avoid this problem, we can linearize SABC^2 and SABC^4. The principle

is based on a Taylor's expansion in the regime $E \ll V$. This asymptotic regime is justified in particular for an harmonic potential $V(x) = \frac{1}{2}x^2$ since V grows quickly as soon as we do not place the boundary too close to the origin and we restrict our computations to relatively not too high energies. For the boundary condition SABC^2 (36), this leads to

$$\partial_{\mathbf{n}}\phi_E = \frac{-1}{\sqrt{\alpha}}\sqrt{V-E}\,\phi_E = -\frac{\sqrt{V}}{\sqrt{\alpha}}\sqrt{1-\frac{E}{V}}\,\phi_E \approx -\frac{\sqrt{V}}{\sqrt{\alpha}}\left(1-\frac{1}{2}\frac{E}{V}\right)\phi_E.$$

Hence, the approximation of SABC^2 is designated by SABC$^2_{\text{lin}}$ and reads

$$\partial_{\mathbf{n}}\tilde{\phi}_E = -\frac{\sqrt{V_{\ell,r}}}{\sqrt{\alpha}}\tilde{\phi}_E + \frac{1}{2}\frac{E}{\sqrt{\alpha}\sqrt{V_{\ell,r}}}\,\tilde{\phi}_E. \tag{39}$$

Next we can isolate the linear part according to E as

$$\partial_{\mathbf{n}}\tilde{\phi}_E = \beta^2_{\ell,r}\tilde{\phi}_E + E\gamma^2_{\ell,r}\tilde{\phi}_E, \tag{40}$$

with $\beta^2_{\ell,r}$ and $\gamma^2_{\ell,r}$ defined by (39). Including these ABCs in the weak formulation (34) leads, after discretization by the $\mathbb{P}_1$ finite element method, to the following linear eigenvalue problem ($M = 2$)

$$\begin{cases} (\alpha\mathbb{S} + \mathbb{M}_V + \mathbb{C}_M)\,\tilde{\boldsymbol{\phi}}^M = \tilde{E}^M(\mathbb{M} + \mathbb{D}_M)\tilde{\boldsymbol{\phi}}^M, \\ \|\mathbb{M}\tilde{\boldsymbol{\phi}}^M\|_2 = 1. \end{cases} \tag{41}$$

We have defined the two matrices ($M = 2$)

$$\mathbb{C}_M = \begin{pmatrix} \alpha\beta^M_\ell & 0 & 0 & 0 \\ 0 & \dots & \dots & 0 \\ 0 & \dots & \dots & 0 \\ 0 & \dots & \dots & 0 \\ 0 & 0 & 0 & \alpha\beta^M_r \end{pmatrix} \tag{42}$$

and

$$\mathbb{B}_M = \begin{pmatrix} -\alpha\gamma^M_\ell & 0 & 0 & 0 \\ 0 & \dots & \dots & 0 \\ 0 & \dots & \dots & 0 \\ 0 & \dots & \dots & 0 \\ 0 & 0 & 0 & -\alpha\gamma^M_r \end{pmatrix}. \tag{43}$$

Problem (41) is directly solved without iteration by using `eigs`. The computational cost is therefore the same as for a Dirichlet boundary condition. Furthermore, since we do not have to iterate, the algorithm provides simultaneously the first p eigenvalues $(\tilde{E}_n^M)_{0\leq n\leq p-1}$ and associated eigenvectors $(\tilde{\boldsymbol{\phi}}_n^M)_{0\leq n\leq p-1}$. The resulting algorithm is called direct. In the case of SABC^4, a similar strategy of linearization of (7) leads to the approximation

$$\partial_{\mathbf{n}}\tilde{\phi}_E = \beta_{\ell,r}^4\tilde{\phi}_E + E\gamma_{\ell,r}^4\tilde{\phi}_E, \tag{44}$$

with $\beta_{\ell,r}^4$ and $\gamma_{\ell,r}^4$ respectively given by

$$\beta_{\ell,r}^4 = \beta_{\ell,r}^2 - \frac{1}{4}\frac{\partial_{\mathbf{n}}V_{|x=x_{\ell,r}}}{V_{\ell,r}} \tag{45}$$

and

$$\gamma_{\ell,r}^4 = \gamma_{\ell,r}^2 - \frac{1}{4}\frac{\partial_{\mathbf{n}}V_{|x=x_{\ell,r}}}{V_{\ell,r}^2} \tag{46}$$

by using the approximation

$$\frac{1}{4}\frac{\partial_{\mathbf{n}}V}{E-V} \approx -\frac{1}{4}\frac{\partial_{\mathbf{n}}V}{V} - \frac{1}{4}\frac{\partial_{\mathbf{n}}V}{V^2}\,E. \tag{47}$$

Adapting the functions, our problem can be written as (41).

4.3. Numerical examples

Example 1 (Harmonic potential). We first consider the well-known (positive) harmonic potential

$$V(x) = \frac{1}{2}x^2, \tag{48}$$

i.e. the equation to solve is

$$-\frac{1}{2}\phi_E'' + \frac{1}{2}x^2\phi_E = E\phi_E, \qquad x\in\mathbb{R}, \tag{49}$$

fixing hence α to $\frac{1}{2}$. The square-integrable normalized solutions of (49) are the *Hermite functions*

$$\phi_n^{\text{ex}}(x) = \frac{\pi^{-1/4}}{\sqrt{2^n n!}}e^{x^2/2}\frac{d^n}{dx^n}\left(e^{-x^2}\right), \quad n\geq 0 \tag{50}$$

and the corresponding eigenvalues (energies) are

$$E_n^{\text{ex}} = n + \frac{1}{2}. \tag{51}$$

The first four eigenfunctions are plotted in Figure 16. More generally, the eigenfunctions $\phi_n^{\text{ex}}(x)$ vanish for $|x| \to \infty$, but this decay is slower and slower as n grows.

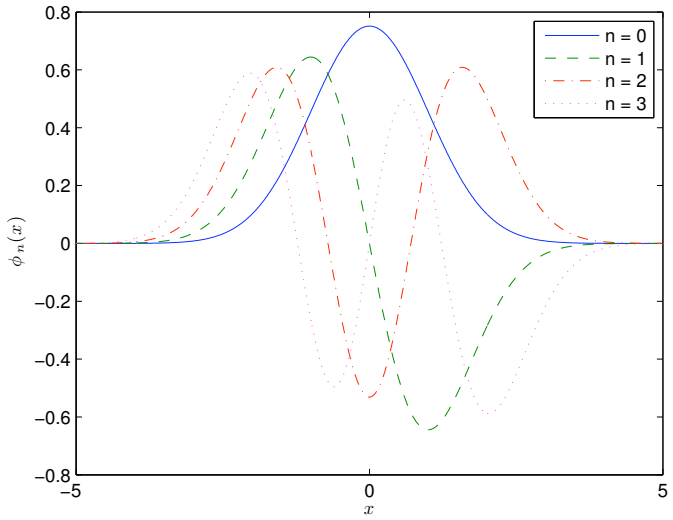

Figure 16: Example 1: The first four eigenfunctions ($n = 0, 1, 2, 3$) associated with the harmonic potential (48).

Let us recall that, for the case of the square-root ABCs, we have the direct and loop strategies. In the sequel, when we present an error calculation with respect to x_r or h, this is clearly obtained by the direct approach since n is fixed. When we compute a range of eigenvalues (curves with n as abscissa), we report the results for both strategies to compare the respective accuracies.

A first numerical test consists in presenting the error on both the energy and eigenfunctions depending on the computational domain size. For the harmonic potential, we always consider a symmetric domain $\Omega =]-x_r; x_r[$. For a fixed n, the value of an eigenfunction is closer to zero as x_r becomes larger. This means that we should observe the impact of the ABCs compared to the homogeneous Dirichlet boundary condition depending on the location of x_r. Figure 17 reports, for the fundamental state $n = 0$ and in logarithmic

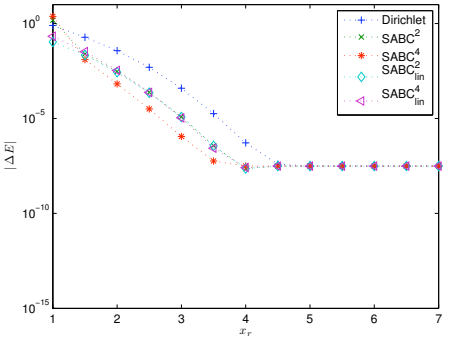

(a) Eigenvalue

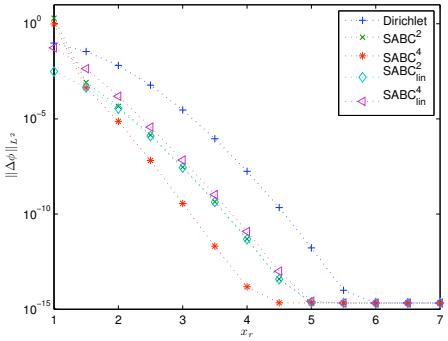

(b) Eigenvector

Figure 17: Example 1: Error ($n = 0$).

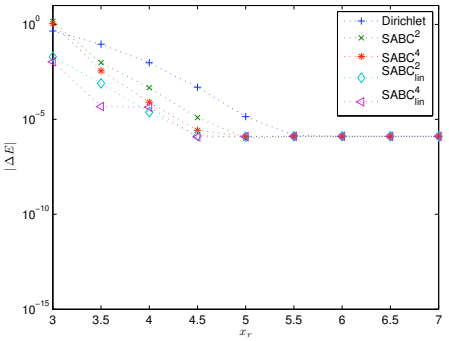

(a) Eigenvalue

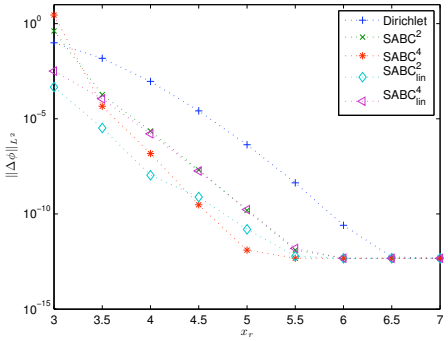

(b) Eigenvector

Figure 18: Example 1: Error ($n = 4$).

scale, the absolute error on the eigenvalue $|\Delta E| = |E_n^{\text{num}} - E_n^{\text{ex}}|$ and the error in the L^2-norm of the eigenfunction $||\Delta\phi||_{L^2(\Omega)} = ||\phi_n^{\text{num}} - \phi_n^{\text{ex}}||_{L^2(\Omega)}$ when the right endpoint x_r varies between 1 and 7. Figure 18 presents similar results for $n = 4$ and x_r varying between 3 and 10. The calculations are obtained for the numerical eigenvalues E_n^{num} equal to E_n^M (for SABC^M) or $\tilde{E}_n^M$ (for SABC$^M_{\text{lin}}$), depending on the order M of the ABC and its type (square-root or linearized). In the nonlinear case, corresponding to SABC^M, the number of iterations is 50 to reach convergence with $\varepsilon = 10^{-12}$. The spatial step size is $h = 1 \cdot 10^{-3}$.

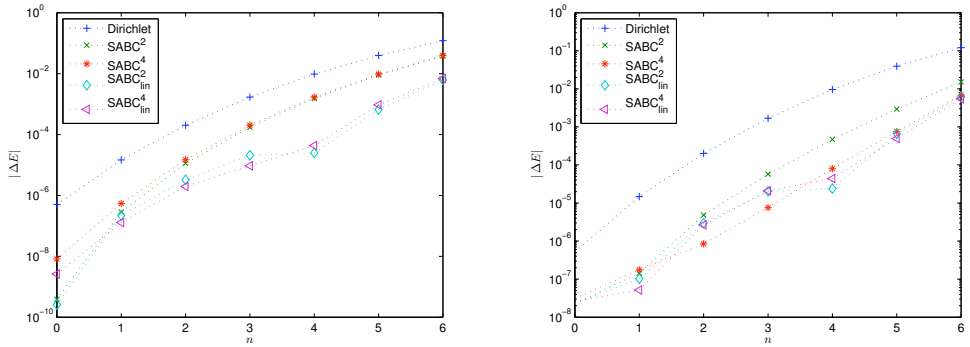

(a) Direct approach

(b) Loop approach

Figure 19: Example 1: Error on the eigenvalue depending on n ($\Omega =]-4; 4[$).

For n fixed, we observe an accuracy improvement for both boundary conditions when x_r grows. When x_r is close to the origin (for example $x_r = 1$ for $n = 0$, $x_r < 3$ for $n = 4$), all the conditions lead to inaccurate results. However, even for these small values of x_r, the linearized ABCs already give an approximation of the eigenvalue while this is not the case for the Dirichlet boundary condition as well as for SABC^{2,4}. Indeed for $x_r = 3$ and $n = 4$, the ABCs SABC$^{2,4}_{\text{lin}}$ give $\tilde{E}_n$ with an error equal to 10^{-2} when the error for the homogeneous Dirichlet boundary condition is about 10^{-1} and 1 for the square-root ABCs. The same remark holds for $n = 0$.

It seems from these tests that the linearized ABCs are the most robust boundary conditions concerning the size of the computational domain. From a general point of view, the ABCs always provide a better precision, at least about the same as with the Dirichlet boundary condition but often far better. The ABCs of different orders generally give a similar accuracy with

however a better accuracy behaviour of the square-root ABCs but at a higher computational cost. They improve the accuracy of the Dirichlet boundary condition from a factor between 10 and 10^3 according to the configuration, before attaining the saturation zone. After a certain value of x_r, all the boundary conditions lead to the same accuracy which only depends on the spatial mesh size. For the computation of the eigenfunctions, this value can be estimated to $x_r = 6$ for $n = 0$ and to $x_r = 6.5$ for $n = 4$.

We also remark that we must increase x_r as n grows to get the same accuracy. To confirm this, we compute the variation of the error when $\Omega =]-x_r; x_r[$ is fixed and n varies. We set $x_r = 4$ and for $n \in [0, 10]$ we report the error on the eigenvalues E_n (Figure 19) for both the "direct" and "loop" approaches. For all the boundary conditions, we can clearly see that the accuracy decays as n increases. Indeed, the ABCs have been built in the high frequency regime. In our context, this means that we require that

$$E_n - V_r \ll 0 \tag{52}$$

holds for a given point x_r and for a fixed potential V. As a consequence, this limits the calculation of energies under the condition $E_n \ll x_r^2/2$ for example in the harmonic case. In the proposed simulation, setting $x_r = 4$ leads to $E_n \ll 8$, which is coherent with the observations in Figure 19. Another way to interpret this property is that increasing the accuracy and the range of eigenvalues must be *a priori* guided by relation (52). To visualize this, we show in Figure 20 the potential V as well as the first energies E_n. We can read from this figure the abscissa x where $E - V$ becomes negative and we can have a first idea of the choice of the minimal abscissa x_r to choose to get a sufficiently large gap between E and $V(x_r)$ according to (52). For example, for the fundamental state $n = 0$, the energy associated with E_0 is the lowest level red curve. From the intersection with the curve of $V(x)$, we can see that $E_0 - V(x)$ is negative for $x \geq 1$ and we can estimate that the difference between E_0 and $V(x)$ will be enough starting from about $x \geq 2$. Coming back to Figure 17 confirms these values since choosing $x_r = 1$ provides a possible computation but does not necessarily converge towards E_0 while setting $x_r = 2$ gives a correct approximation of E_0. We can do the same analysis for $n = 4$ (fifth red curve from the bottom). We see that $E_4 - V(x)$ is negative from $x \geq 3$ and "very negative" after $x \geq 4$. These values must be connected with the curves of Figure 18.

On this example ($n = 4$), we also remark that the linearized ABCs are more accurate than the original square-root ABCs, with a gain of a fac-

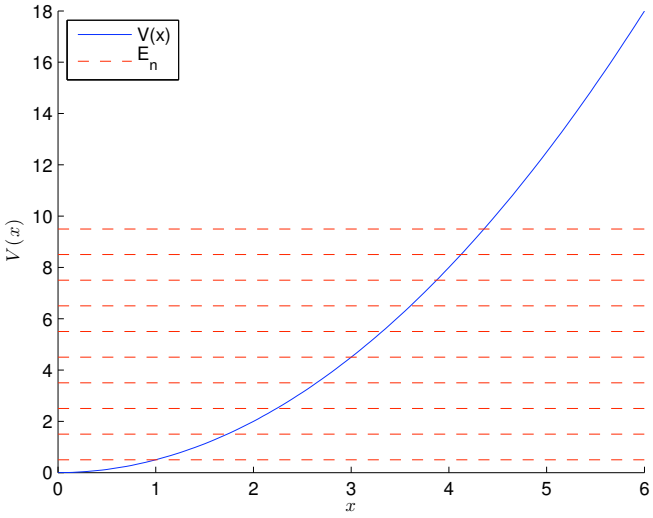

Figure 20: Example 1: Harmonic potential and the energies E_n for $0 \leq n \leq 9$.

tor 10 in precision. This remark could also have been made on Figure 18 corresponding to $n = 4$, most particularly for the computation of the eigenvalue. The precision obtained for $x_r \geq 4.5$ with the linearized boundary conditions is the same as for the square-root boundary conditions but the linearization yields an accuracy improvement on smaller computational domains while the iterative algorithm for the square-root conditions does not converge ($2 \leq x_r \leq 3$). Moreover, let us note that the spectrum is simultaneously obtained in the linear case without iterating which is a crucial gain compared to the "loop" approach, showing hence the need of linearizing. As a consequence, the ABCs $\text{SABC}^M_{\text{lin}}$ are, for a similar computational cost, to privilege to the Dirichlet boundary condition for accuracy purpose and/or for reducing the computational domain. Let us also finally remark that the gain in terms of accuracy of the "loop" approach is interesting as we can see it in Figure 18(a) but for a relatively higher computational complexity.

We now wish to compare the performances of the linearized and square-root ABCs. The previous curves illustrated the question of accuracy. Generally speaking, the square-root ABCs provide a better accuracy but at a higher computational cost even for the "direct" approach since a fixed point is required. We show in Figure 21 the number of iterations when using SABC^2 and SABC^4, with respect to x_r, for two situations: $n = 0$ and $n = 4$. Fig-

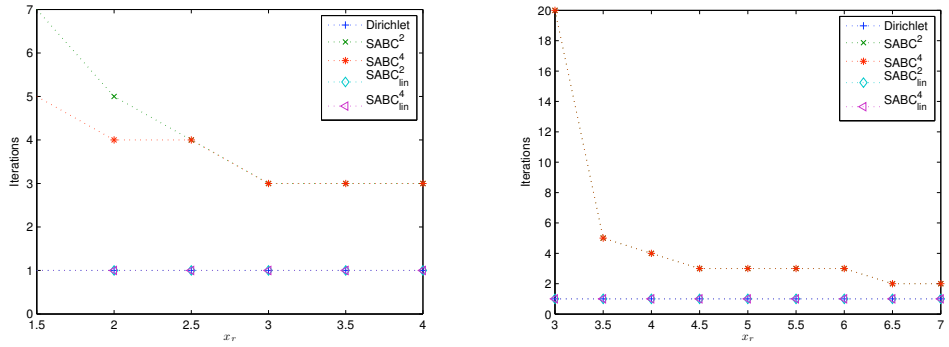

(a) $n = 0$ (b) $n = 4$

Figure 21: Example 1: Number of iterations needed for the algorithms associated with the different ABCs, with respect to x_r for $n = 0$ and $n = 4$.

ures 21(a) and 21(b) must be connected to Figures 17 and 18 which are their equivalent in terms of accuracy. For the first value of x_r, we often observe the divergence of the algorithm (the maximal number of iterations of the fixed point algorithm is 20). Again, this is one of the interesting property of the linear ABCs since, if we go back to Figures 17 and 18, they also give a rough estimate of the eigenvalue. For a slightly larger value of x_r, the number of iterations stagnates to 5. Finally, when the maximal accuracy is reached, the algorithm needs 2 or 3 iterations. Globally, the computational costs for the square-root ABCs are roughly 5 times the costs for the linear ones and the Dirichlet boundary condition. At the same time, a higher accuracy is obtained.

Finally, we present in Figures 22 ($n = 0$) and 23 ($n = 4$) the influence of the discretization on the accuracy for a given domain $]-x_r; x_r[$. We fix x_r and report the errors $|\Delta E|$ and $\|\Delta\phi\|_{L^2(\Omega)}$ depending to the mesh size h, for h between $h = 5 \cdot 10^{-2}$ and $h = 1 \cdot 10^{-4}$. The value of x_r is chosen such that the saturation of the error has not been reached yet so that we can see an effect of the ABCs compared to the Dirichlet boundary condition. One remarkable property is that for $n = 0$ (Figure 22) the accuracy remains increasing with the ABCs by refining the mesh while this is not the case for the Dirichlet boundary condition. Indeed, we cannot gain more accuracy after $h = 10^{-2}$ if we do not increase the size of the computational domain. Concerning the ABCs (which are already more accurate than the Dirichlet boundary condition for $h = 10^{-2}$), we can still improve the solution by refining, most

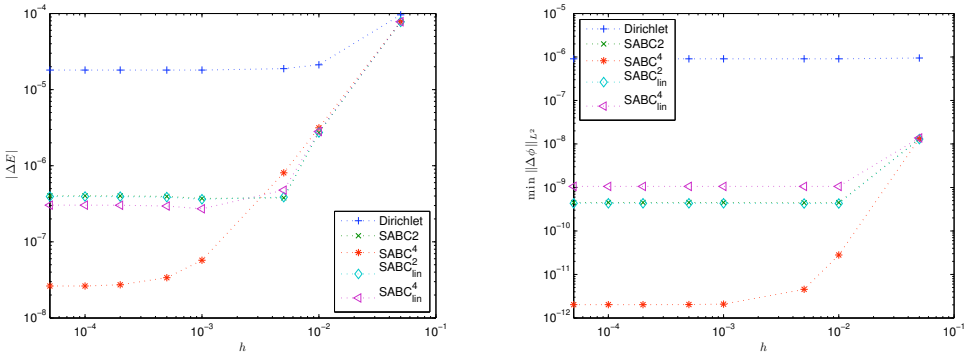

(a) Eigenvalue (b) Eigenfunction

Figure 22: Example 1: Error ($x_r = 3.5$ and $n = 0$) with respect to h.

particularly with SABC^4. This remark holds for both the eigenvalues and eigenvectors.

Example 2 ('Double-well" potential). Let us now consider other potentials like the so-called "double-well" potential

$$V(x) = \frac{1}{2}(1 - x^2)^2 \tag{53}$$

which is drawn in Figure 24(a). In this situation, we have $\alpha = \frac{1}{2}$ in (29). The energy of the fundamental state is [23]

$$E \approx 0.56889338. \tag{54}$$

and is presented in Figure 24(b), superposed to the potential. We can directly see the high-frequency assumption $E \ll (1 - x_r^2)^2/2$. For $x_r = 1.5$, we find $(1 - x_r^2)^2/2 \approx 0.78$ and $(1 - x_r^2)^2/2 = 4.5$ for $x_r = 2$. Then we have to choose $x_r \geq 2$ to get a good accuracy. We can observe this condition in Figure 25 which presents the error on this eigenvalue for each boundary condition depending to the domain size (position of x_r). As the harmonic potential, the error decays as the size of the domain increases. The ABCs can be ordered as previously with a much better accuracy than with the Dirichlet boundary condition, most particularly for the linearized ABCs for the same computational cost. For $x_r = 1.5$, we remark that all the conditions lead to a wrong computation of E. As soon as the high frequency assumption is fulfilled for $x_r = 2$, then we have a good error precision.

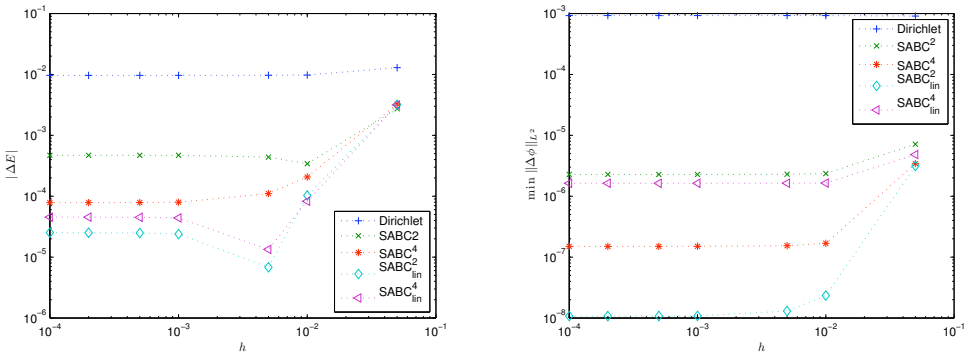

(a) Eigenvalue (b) Eigenfunction

Figure 23: Example 1: Error ($x_r = 4$ and $n = 4$) with respect to h.

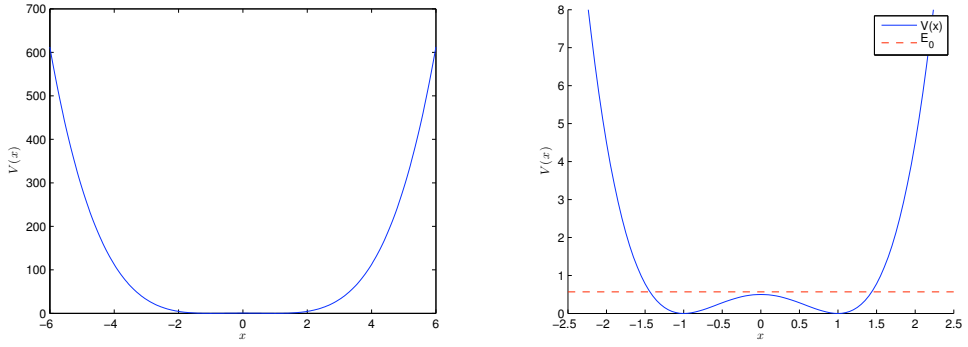

(a) Potential (b) Fundamental energy

Figure 24: Example 2: The "double-well" potential and its fundamental energy.

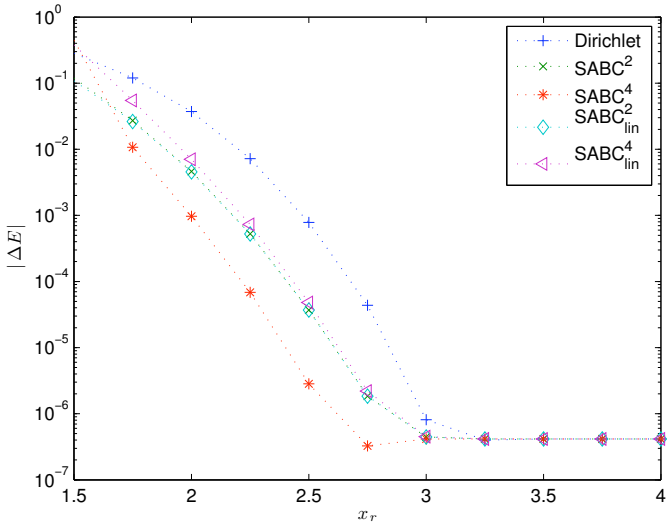

Figure 25: Example 2: Error on the first eigenvalue for the "double-well" potential ($h = 10^{-3}$).

The three potentials that we analyze now have all the property to lead to negative eigenvalues. A necessary condition to justify the application of the previous approach is that

$$V(x_r) - E \geq 0. \tag{55}$$

Hence, according to n and the rank of the eigenvalue that we are looking for, we have to choose x_r sufficiently large so that condition (55) is fulfilled. Since V is negative and even if we have $E \ll V$, then linearizing SABC^{2,4} by using a Taylor's expansion with respect to E/V is no longer relevant since V can be equal to zero. Let us set $V_{\min} = \min_{x\in\mathbb{R}} V(x)$ and using the property that the Schrödinger equation is linear, we define a new positive potential $W = V - V_{\min}$ and $F_n = E_n - V_{\min}$. Problem (29)–(30) is then equivalent to

$$-\alpha\phi_E'' + W\phi_E = F_n\phi_E. \tag{56}$$

The boundary conditions SABC$^{2,4}_{\text{lin}}$ are so the linearized versions of SABC^{2,4} according to $1/(V - V_{\min})$ (and not $1/V$) by using the equivalent assumption

$$E - V_{\min} \ll V - V_{\min}. \tag{57}$$

Example 3 (Pöschl-Teller potential). The *Pöschl-Teller potential* [24] is given by

$$V(x) = -\frac{\lambda(\lambda+1)}{\cosh^2(x)}, \tag{58}$$

and $\alpha = 1$ in (29). This potential is always negative (see Figure 26(a)). For $\lambda = 9$, it leads to nine eigenvalues

$$E_n = -(9-n)^2, \quad 0 \leq n \leq 8. \tag{59}$$

In Figure 26(b), we plot the different energy levels, compared to the potential. To take into account the translation, we rather present $V(x) - V_{\min}$ and $E_n - V_{\min}$. For a given eigenstate, we can *a priori* estimate the size of the computational domain to consider that the high frequency hypothesis is satisfied and that the convergence of the iterative algorithm occurs. We set $h = 5 \cdot 10^{-4}$ and analyze, for n fixed, $0 \leq n \leq 8$, the error on E_n for the different ABCs depending on the position of x_r. We depict the results in Figure 26 for $n = 0$, $n = 4$ and $n = 8$. The ABCs always improve the accuracy compared to the Dirichlet boundary condition. This is most particularly clear for large n. For $n = 8$ and $]-5;5[$, the accuracy obtained with the Dirichlet boundary condition is less than 10^{-2} and about $5 \cdot 10^{-5}$ for $\text{SABC}^{2,4}$. To get a similar precision with the Dirichlet boundary condition, we would have to choose $x_r = 10$ leading therefore to a significant larger computational domain. The effect of the linearized ABCs is variable. For $n = 0$ the ABCs $\text{SABC}^{2,4}_{\text{lin}}$ are almost as precise as the ABCs $\text{SABC}^{2,4}$, but when n increases, the accuracy is similar to the one obtained by using the Dirichlet boundary condition.

For the same potential, we observe in Figure 28 the error on E_n for x_r fixed. For $x_r = 2$, we notice a factor 10 to 100 between the Dirichlet boundary condition and the ABCs for the states $2 \leq n \leq 6$. The second- and fourth-order ABCs have a similar accuracy. At $x_r = 4$, all the boundary conditions are equivalent for the first eigenstates but when n grows the ABCs remain accurate while the Dirichlet boundary condition is less precise ($n = 6$, $n = 7$). Indeed, they yield an accuracy of the eigenvalue about 10^{-3} while the Dirichlet boundary condition gives only 10^{-1} ($n = 8$).

Example 4 (Woods-Saxon potential). The *Woods-Saxon potential* reads

$$V(x) = c_0 z(x) \left[1 - a(1 - z(x))\right], \quad x \in [0, +\infty[, \tag{60}$$

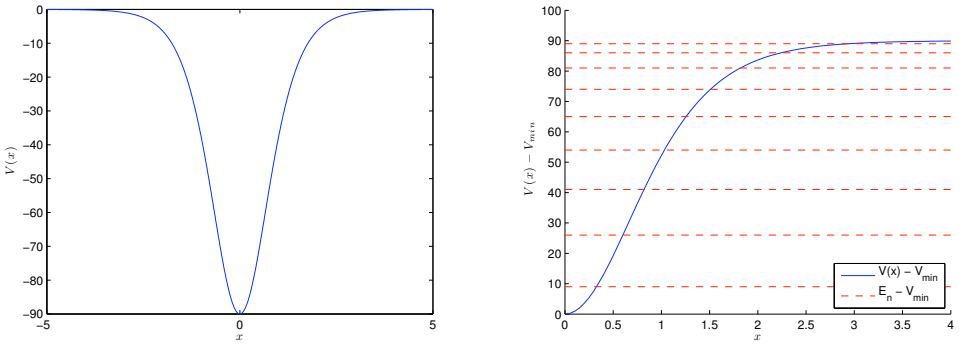

(a) Pöschl-Teller potential (b) Energy levels

Figure 26: Example 3: Pöschl-Teller potential and its first nine energy levels.

with

$$z(x) = \frac{1}{e^{a(x-b)} + 1},$$

and setting the parameters $c_0 = -50$, $a = 5/3$, $b = 7$. The coefficient α in (29) is equal to 1. For this potential [24], the first 14 eigenvalues of H are negative and given by (with a round-off error equal to 10^{-15})

$$\begin{aligned}
E_1 &= -49.457788728082580 & E_8 &= -30.912247487908848 \\
E_2 &= -48.148430420006361 & E_9 &= -26.873448916059872 \\
E_3 &= -46,290753954466088 & E_{10} &= -22.588602257693220 \\
E_4 &= -43.968318431814233 & E_{11} &= -18.094688282124421 \\
E_5 &= -41.232607772180218 & E_{12} &= -13.436869040250077 \\
E_6 &= -38.122785096727920 & E_{13} &= -8.676081670736546 \\
E_7 &= -34.672313205699651 & E_{14} &= -3.908232481206230
\end{aligned}$$

The Woods-Saxon potential is only defined for some positive values of x. For this reason, we select the computational domain $[0; x_r]$. At $x_\ell = 0$, we impose the homogeneous Dirichlet boundary condition $\phi(0) = 0$. We present this potential and its energy levels $E_n - V_{\min}$ compared to $V(x) - V_{\min}$ in Figure 29.

Figure 30 shows for $n = 3$ and $n = 14$ the error on the eigenvalues when we move the right endpoint x_r. We consider $h = 5 \cdot 10^{-4}$. Independently of the eigenstate, the ABCs improve clearly the results obtained by using the

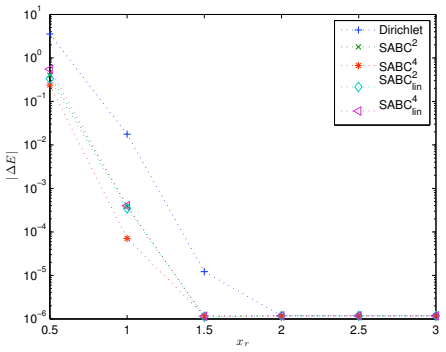

(a) $n = 0$

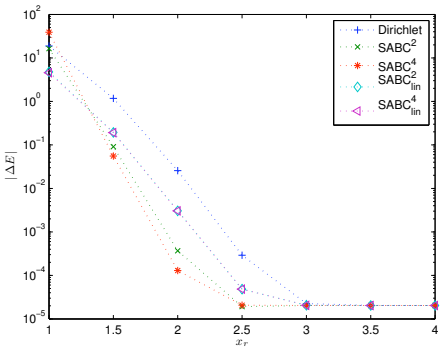

(b) $n = 4$

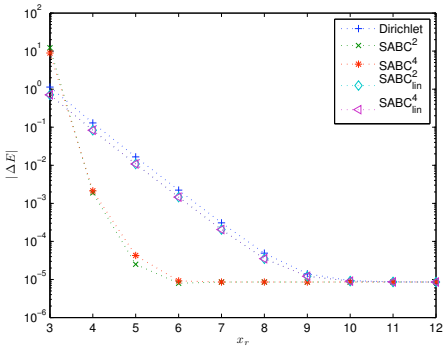

(c) $n = 8$

Figure 27: Example 3: Error of the eigenvalues for the different ABCs and the Pöschl-Teller potential.

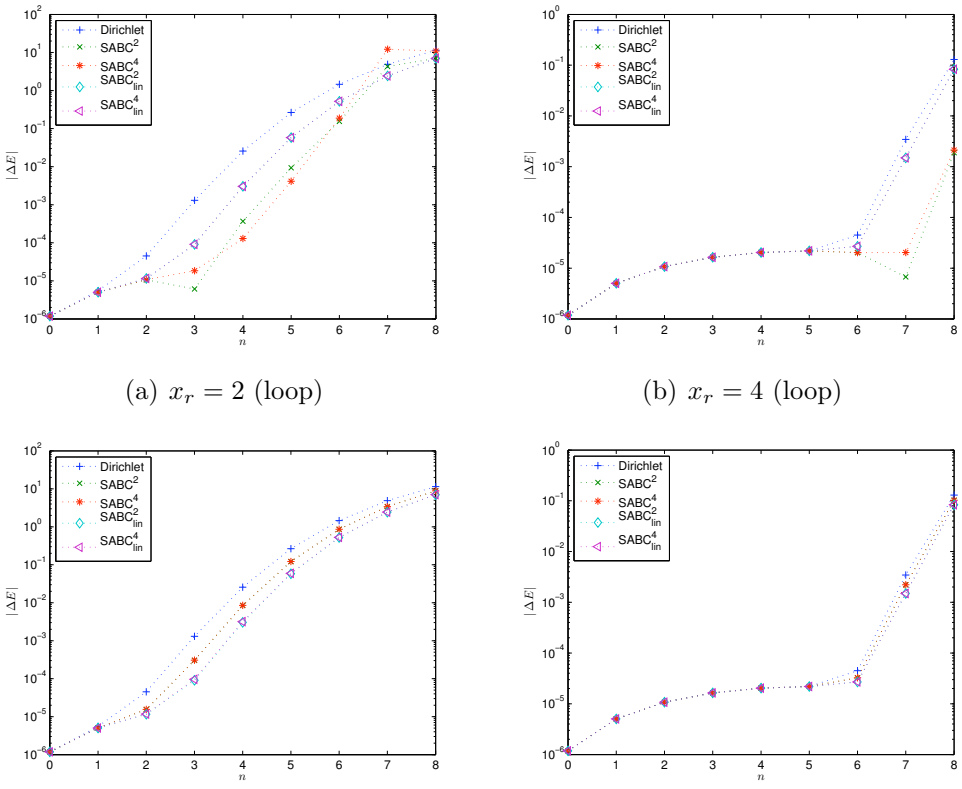

(a) $x_r = 2$ (loop) (b) $x_r = 4$ (loop)

(c) $x_r = 2$ (direct) (d) $x_r = 4$ (direct)

Figure 28: Example 3: Error on the eigenvalues according to n for the Pöschl-Teller potential.

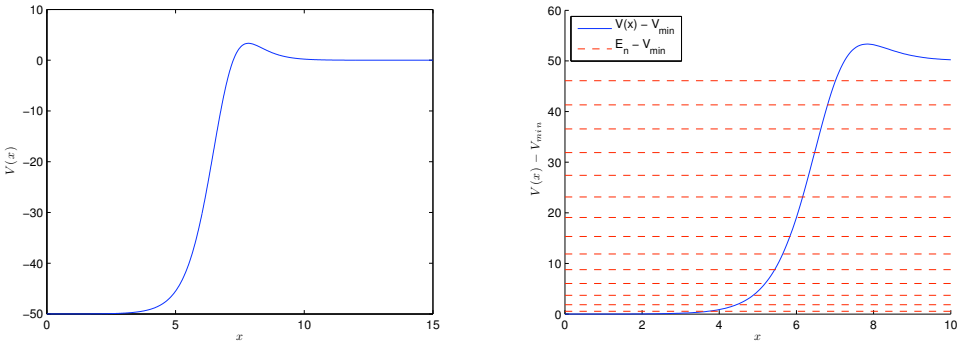

(a) Potential (b) Energy levels

Figure 29: Example 4: The Woods-Saxon potential and its energy levels.

Dirichlet boundary condition. For $n = 3$, the fourth-order ABC seems to lead to the best results compared to the second-order ABC. However, the case $n = 14$ does not confirm this. Concerning the linearized ABCs, their effect is variable. For $n = 3$, we get the same accuracy between the linearized and original square-root ABCs for a fixed order. For $n = 14$, the linearized ABCs are slightly better than the Dirichlet boundary condition and clearly much less accurate than their square-root versions. However, the extreme point $x_r = 7$ is an exception since the iterative algorithm does not converge while the linearized ABCs provide an approximate value of E_{14} with an error of 0.5.

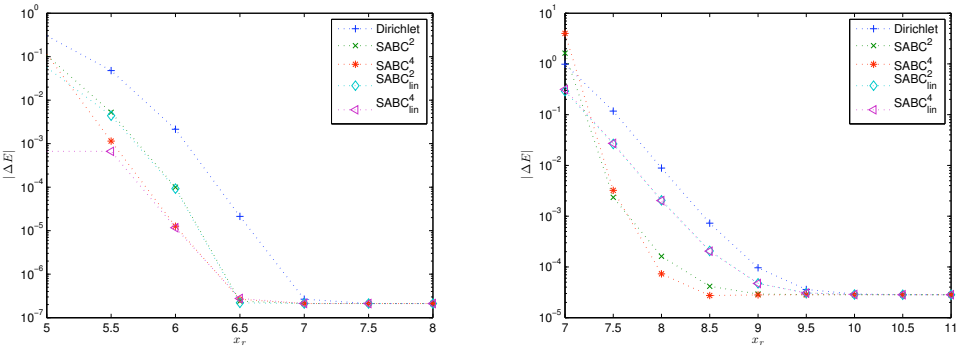

(a) $n = 3$ (b) $n = 14$

Figure 30: Example 4: Woods-Saxon potential depending on x_r for n fixed.

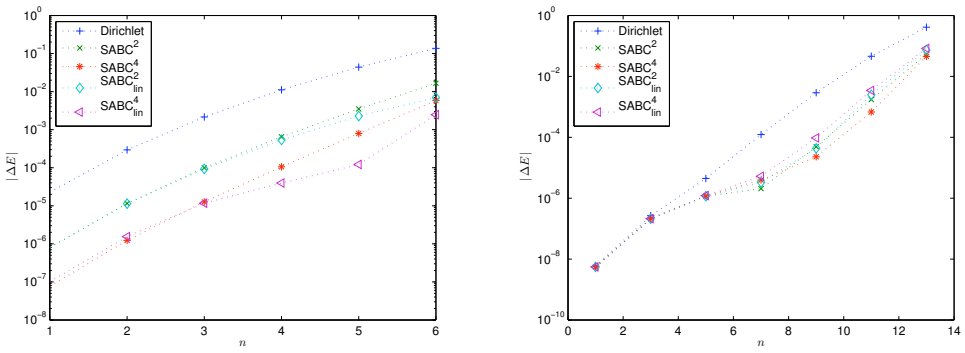

(a) $x_r = 6$ (b) $x_r = 7$

Figure 31: Example 4: Woods-Saxon potential with respect to n for x_r fixed (loop).

Let us now analyze the accuracy with respect to the eigenstate for a given computational domain (see Figure 31). This confirms the previous remarks, in particular concerning the accuracy improvement when considering an ABC. Moreover, the fourth-order ABC always lead to at least the same precision as the second-order ABC. This can be seen for $x_r = 6$ since we have a factor about 10 between the two ABCs. These computations are done with the loop approach. The linearized ABCs yield a clear improvement of the results compared with the Dirichlet boundary condition at the same computational cost.

Example 5 (Morse potential). Finally, we consider the *Morse potential* [24]

$$V(x) = D_e \left[(1 - e^{-\beta(x - x_e)})^2 - 1 \right], \tag{61}$$

with $\alpha = 1$ in (29). The constant D_e is called the dissociation energy, x_e is the equilibrium internuclear distance and β is a disposable parameter. The numerical values are $D_e = 605559/1000$, $x_e = 240873/100000$, $\beta = 988879/1000000$. The n-th exact eigenvalue is given by

$$E_n = -\beta^2 \left(\frac{\sqrt{D_e}}{\beta} - \left(n - \frac{1}{2} \right) \right)^2, \quad n \geq 1. \tag{62}$$

This potential and its energy levels are shown in Figure 32.

For the numerical study, we set $h = 5 \cdot 10^{-4}$ and present the error depending on x_r (Figure 33(a)) or n (Figure 33(b)). For this potential, the

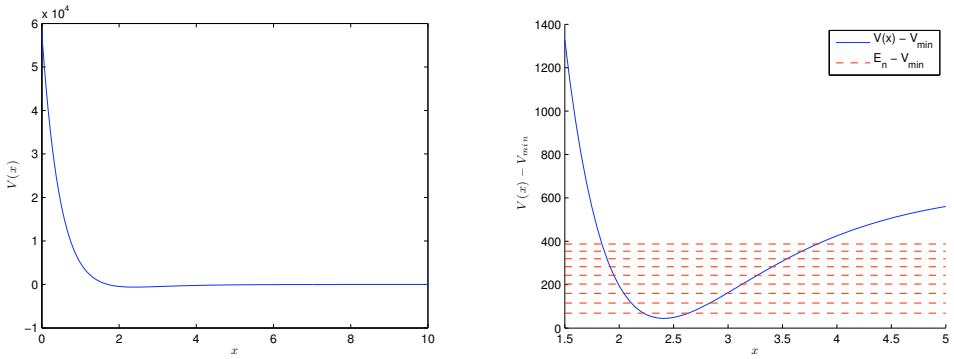

(a) Potential (b) Energy levels

Figure 32: Example 5: The Morse potential and its energy levels.

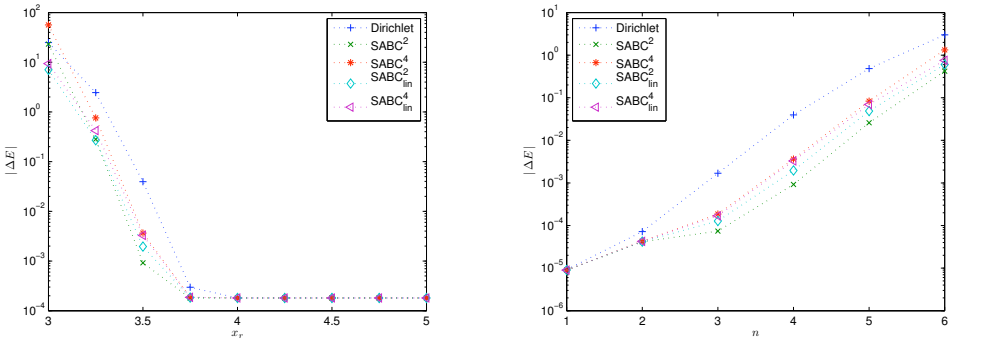

(a) Error according to x_r, for $n = 4$ (b) Error according to n, for $x_r = 3.5$ (loop)

Figure 33: Example 5: Morse potential.

difference is less visible than in the other examples, the most accurate approach being the loop approach for SABC^{2,4}. Nevertheless, the approach based on the ABCs is always at least as accurate as the one with a Dirichlet boundary condition, with sometimes an improvement factor between 10 and 100 in some zones. We can remark that this holds for the linearized ABCs too. The plot of the energy levels in Figure 32 allows to adjust the size of the computational domain.

5. Application to the computation of ground states: the nonlinear case

5.1. Problem and numerical scheme

We are interested in computing ground states for nonlinear Schrödinger equations. Most particularly, we consider a nonlinear potential which is the sum of a cubic nonlinearity and a harmonic potential. This kind of nonlinearity arises e.g. in Bose-Einstein condensates [25, 26, 27]. The dimensionless *one-dimensional Gross-Pitaevskii equation* [23, 28, 29] reads

$$i\frac{\partial\psi}{\partial t} = -\frac{1}{2}\partial_x^2\psi + V\psi + \beta|\psi|^2\psi, \qquad x \in \mathbb{R}, \tag{63}$$

setting $V(x) = \frac{1}{2}x^2$ and where the nonlinearity coefficient β can be negative or positive. We restrict ourselves to this special nonlinearity but all results can be directly extended to other cases. In view of computing the stationary solutions we write

$$\psi(x,t) = e^{-iEt}\phi_E(x), \tag{64}$$

where E is the chemical potential of the condensate and ϕ_E is a real-valued function independent of time. Let us note that the stability of exactly this kind of problems was studied analytically in [30, 31, 32] and hence can be checked numerically using our proposed ABCs.

Function ϕ_E is then solution to

$$-\alpha\partial_x^2\phi_E + V\phi_E + \beta\left|\phi_E\right|^2\phi_E = E\phi_E, \qquad x \in \mathbb{R}, \tag{65}$$

where $\alpha = \frac{1}{2}$, under the *normalization constraint*

$$\|\phi_E\|_{L^2(\mathbb{R})} = 1. \tag{66}$$

Finally, the function ϕ_E of the problem (65)–(66) satisfies the boundary conditions $\phi_E'(0) = 0$ and $\phi_E(\pm x) \to 0$ for $x \to +\infty$. The resulting system is a nonlinear eigenvalue problem under constraint. The eigenfunction ϕ_E being known, we can determine the associated eigenvalue E by

$$E = \int_{\mathbb{R}} \alpha\left|\partial_x\phi_E\right|^2 + V\phi_E^2 + \beta\phi_E^4\, dx. \tag{67}$$

The problem (65)-(66) is solved on a symmetric computational domain $\Omega =]-R; R[$, with $R > 0$ and $\Sigma = \{-R; R\}$. We keep on denoting this domain

by $\Omega =]-x_\ell; x_r[$. We introduce (E^0, ϕ^0) as a solution to the boundary value problem with Dirichlet boundary condition

$$\begin{cases} -\alpha\partial_x^2\phi_E + V\phi_E + \beta|\phi_E|^2\phi_E = E\phi_E, & \text{in } \Omega, \\ \phi_E = 0, & \text{on } \Sigma, \\ \|\phi_E\|_{L^2(\Omega)} = 1. \end{cases} \tag{68}$$

Analogously, we designate by (E^M, ϕ^M) the solution computed with a M-th order nonlinear ABC obtained from the linear stationary ABCs (6)–(7). To this end, we replace formally the potential V by the new nonlinear potential $V + \beta|\phi|^2$ to get the second-order ABC

$$\partial_{\mathbf{n}}\phi_E = \frac{i}{\sqrt{\alpha}}\sqrt{E - V - \beta|\phi_E|^2}\,\phi_E, \quad \text{on } \Sigma, \tag{69}$$

and fourth-order ABC

$$\partial_{\mathbf{n}}\phi_E = \frac{i}{\sqrt{\alpha}}\sqrt{E - V - \beta|\phi_E|^2}\,\phi_E + \frac{1}{4}\frac{\partial_{\mathbf{n}}(V + \beta|\phi_E|^2)}{E - V - \beta|\phi_E|^2}\,\phi_E, \quad \text{on } \Sigma. \tag{70}$$

For the sake of clarity, we keep on designating by SABC^M the above M-th order ABC.

The interior equation is discretized by the *semi-implicit scheme*

$$-\alpha\partial_x^2\phi^{M,j+1} + V\phi^{M,j+1} + \beta|\phi^{M,j}|^2\phi^{M,j+1} = E^{M,j+1}\phi^{M,j+1}, \tag{71}$$

for $j \geq 0$ and $M = 0, 2, 4$. Now and independently of the boundary condition, the algorithm must be iterative since the interior scheme is nonlinear. As a consequence, we systematically use the fixed point method on the n-th eigenvalue E_n^M and eigenfunction ϕ_n^M for solving the eigenvalue problem. The variational formulation reads

$$\begin{aligned} -\alpha[\partial_{\mathbf{n}}\phi_n^{M,j+1}\psi]_{x_\ell}^{x_r} + \alpha\int_\Omega \partial_x\phi_n^{M,j+1}\partial_x\psi dx + \int_\Omega V\phi_n^{M,j+1}\psi dx \\ + \beta\int_\Omega |\phi_n^{M,j}|^2\phi_n^{M,j+1}\psi dx = E_n^{M,j+1}\int_\Omega \phi_n^{M,j+1}\psi dx, \end{aligned} \tag{72}$$

for any test-function ψ. In the Dirichlet case, by choosing $\psi \in H_0^1(\Omega)$, which makes the first term of the equation vanish, the discrete problem is, for $M = 0$,

$$\begin{cases} \left(\alpha\mathbb{S}^0 + \mathbb{M}_V^0 + \beta\mathbb{M}_{|\boldsymbol{\phi}_n^{M,j}|^2}^0\right)\boldsymbol{\phi}_n^{M,j+1} = E_n^{M,j+1}\mathbb{M}^0\boldsymbol{\phi}_n^{M,j+1}, \\ \|\mathbb{M}^0\boldsymbol{\phi}_n^{M,j+1}\|_2 = 1. \end{cases} \tag{73}$$

For the ABCs, we use for $\partial_{\mathbf{n}}\phi_n^{M,j+1}$ the fixed point version

$$\partial_{\mathbf{n}}\phi_n^{M,j+1} = \frac{i}{\sqrt{\alpha}}\sqrt{E_n^{M,j} - V - \beta|\phi_n^{M,j}|^2}\,\phi_n^{M,j+1} \tag{74}$$

for the second-order ABC (69) and

$$\partial_{\mathbf{n}}\phi_n^{M,j+1} = \left(\frac{i}{\sqrt{\alpha}}\sqrt{E_n^{M,j} - V - \beta|\phi_n^{M,j}|^2} + \frac{1}{4}\frac{\partial_{\mathbf{n}}(V+\beta|\phi_n^{M,j}|^2)}{E_n^{M,j} - V - \beta|\phi_n^{M,j}|^2}\right)\phi_n^{M,j+1} \tag{75}$$

for the fourth-order condition (70). Hence, the term $-\alpha[\partial_{\mathbf{n}}\phi_n^{M,j+1}\varphi]_{x_\ell}^{x_r}$ leads, from a discrete point of view, to a matrix contribution $\mathbb{B}_M^j\boldsymbol{\phi}^{M,j+1}$ for the M-th order ABC, where the matrix coefficients $\mathbb{B}_M^j$ only depend on the values of $\boldsymbol{\phi}_n^{M,j}$ and $E_n^{M,j}$. By applying the fixed point algorithm on the n-th eigenvalue E_n^M and eigenvector leads to the iterative scheme $\boldsymbol{\phi}_n^M$

$$\begin{cases} \left(\alpha\mathbb{S} - \alpha\mathbb{B}^{M,j} + \mathbb{M}_V + \beta\mathbb{M}_{|\boldsymbol{\phi}_n^{M,j}|^2}\right)\boldsymbol{\phi}_n^{M,j+1} = E_n^{M,j+1}\mathbb{M}\boldsymbol{\phi}_n^{M,j+1}, \\ \|\mathbb{M}\boldsymbol{\phi}_n^{M,j+1}\|_2 = 1. \end{cases} \tag{76}$$

The matrix coefficients $\mathbb{B}^{M,j}$ are given by

$$(\mathbb{B}^{M,j})_{1,1} = \frac{i}{\sqrt{\alpha}}\sqrt{E_n^{M,j} - V_\ell - \beta|\boldsymbol{\phi}_{n,\ell}^{M,j}|^2} + \frac{1}{4}\frac{\partial_{\mathbf{n}}(V+\beta|\boldsymbol{\phi}_n^{M,j}|^2)_{|x=x_\ell}}{E_n^{M,j} - V_\ell - \beta|\boldsymbol{\phi}_{n,\ell}^{M,j}|^2} \tag{77}$$

and

$$(\mathbb{B}^{M,j})_{n_h+1,n_h+1} = \frac{i}{\sqrt{\alpha}}\sqrt{E_n^{M,j} - V_r - \beta|\boldsymbol{\phi}_{n,r}^{M,j}|^2} + \frac{1}{4}\frac{\partial_{\mathbf{n}}(V+\beta|\boldsymbol{\phi}_n^{M,j}|^2)_{|x=x_r}}{E_n^{M,j} - V_r - \beta|\boldsymbol{\phi}_{n,r}^{M,j}|^2} \tag{78}$$

for SABC^4 ($M=4$). For SABC^2 ($M=2$), it is sufficient to retain only the first term of each of the above expressions. We have set here: $\boldsymbol{\phi}_{n,\ell}^{M,j} = \boldsymbol{\phi}_{n,|x=x_\ell}^{M,j}$ and $\boldsymbol{\phi}_{n,r}^{M,j} = \boldsymbol{\phi}_{n,|x=x_r}^{M,j}$.

As in the linear case, we can formulate the linearized versions of the second- and fourth-order ABCs. These ABCs are then designated by SABC$_{\text{lin}}^{2,4}$. Doing so, we have the second-order ABC

$$\partial_{\mathbf{n}}\phi_n^{M,j+1} = -\frac{\sqrt{V}}{\sqrt{\alpha}}\phi_n^{M,j+1} - \frac{\beta}{2}\frac{1}{\sqrt{\alpha}\sqrt{V}}|\phi_n^{M,j}|^2\phi_n^{M,j+1} + \frac{1}{2}\frac{1}{\sqrt{\alpha}\sqrt{V}}E_n^{M,j+1}\phi_n^{M,j+1} \tag{79}$$

and the fourth-order ABC

$$\begin{aligned}\partial_{\mathbf{n}}\phi_n^{M,j+1} = &-\frac{\sqrt{V}}{\sqrt{\alpha}}\phi_n^{M,j+1} - \frac{\beta}{2}\frac{1}{\sqrt{\alpha}\sqrt{V}}|\phi_n^{M,j}|^2\phi_n^{M,j+1} + \frac{1}{2}\frac{1}{\sqrt{\alpha}\sqrt{V}}E_n^{M,j+1}\phi_n^{M,j+1}\\ &+\left(-\frac{1}{4}\frac{\partial_{\mathbf{n}}(V+\beta|\phi_n^{M,j}|^2)}{V} + \frac{\beta}{4}\frac{|\phi_n^{M,j}|^2\partial_{\mathbf{n}}(V+\beta|\phi_n^{M,j}|^2)}{V^2}\right)\phi_n^{M,j+1}\\ &- E_n^{M,j+1}\frac{\partial_{\mathbf{n}}(V+\beta|\phi_n^{M,j}|^2)}{V^2}\phi_n^{M,j+1}.\end{aligned} \tag{80}$$

The iterative scheme then reads

$$\begin{cases}\left(\alpha\mathbb{S} - \alpha\mathbb{B}^{M,j} + \mathbb{M}_V + \beta\mathbb{M}_{|\boldsymbol{\phi}_n^{M,j}|^2}\right)\boldsymbol{\phi}_n^{M,j+1} = E_n^{M,j+1}\left(\mathbb{M} + \alpha\mathbb{B}_{E,M}^{j}\right)\boldsymbol{\phi}_n^{M,j+1}\\ \|\mathbb{M}\boldsymbol{\phi}_n^{M,j+1}\|_2 = 1.\end{cases} \tag{81}$$

The matrix coefficients $\mathbb{B}^{M,j}$ et $\mathbb{B}_E^{M,j}$ are given by

$$\begin{aligned}(\mathbb{B}^{M,j})_{1,1} = &-\frac{\sqrt{V_\ell}}{\sqrt{\alpha}} - \frac{\beta}{2}\frac{1}{\sqrt{\alpha}\sqrt{V_\ell}}|\phi_{n,\ell}^{M,j}|^2\\ &- \frac{1}{4}\frac{\partial_{\mathbf{n}}(V_\ell+\beta|\phi_{n,\ell}^{M,j}|^2)}{V_\ell} + \frac{\beta}{4}\frac{|\phi_{n,\ell}^{M,j}|^2\partial_{\mathbf{n}}(V_\ell+\beta|\phi_{n,\ell}^{M,j}|^2)}{V_\ell^2}\end{aligned} \tag{82}$$

and

$$(\mathbb{B}_E^{M,j})_{1,1} = \frac{1}{2}\frac{1}{\sqrt{\alpha}\sqrt{V_\ell}} - \frac{\partial_{\mathbf{n}}(V_\ell+\beta|\phi_{n,\ell}^{M,j}|^2)}{V_\ell^2} \tag{83}$$

for the fourth-order ABC. The expression of the coefficients of index $(n_h + 1, n_h + 1)$ is the same but taking its value at $x = x_r$. Finally, we can easily extract the coefficients associated with the second-order ABC by keeping only the first term of each expression. Unlike the linear situation, there is no gain in terms of computational time here since the problem is fully nonlinear.

5.2. Numerical results

We consider (65) for different values of the parameter β. For each value, we uniquely determine the fundamental state $n = 0$, see Figure 34. In Table 1 we report the values from [28]. However, these approximate eigenvalues have a limited accuracy. To have some new reference values, we numerically compute them on the domain $]-30; 30[$, with a discretization step $h = 10^{-4}$

and SABC^2 (70). This method provides some new values reported in Table 2 which are conform with Table 1. Let us note here that we do not give some results for larger values of β because the fixed point algorithm then diverges. It would be necessary at this point to use another numerical algorithm (a Newton method or a continuation method) for solving the problem with an ABC. Finally, we present in the sequel the absolute errors: $\Delta E = |E^{\text{num}} - E^{\text{ref}}|$ and $\Delta\phi(0) = |\phi^{\text{num}}(0) - \phi^{\text{ref}}(0)|$, where 'ref' refers to the values in Table 2 and 'num' to the ones computed with the proposed method.

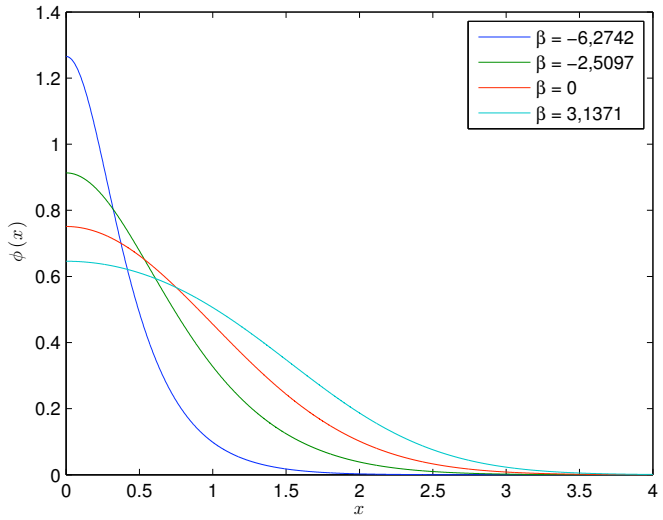

Figure 34: Eigenfunctions (for $x_r = 4$).

β	$\phi_E(0)$	E
-12.5484	1.7718	-19.669
-6.2742	1.2654	-4.9553
-2.5097	0.9132	-0.8061
0	0.7511	0.5000
3.1371	0.6459	1.5265

Table 1: Numerical values E^{ref} and $\phi_E^{\text{ref}}(0)$ from [28] depending on β.

For the simulations, the initialization of the fixed point algorithm uses

β	$\phi_E(0)$	E
-12.5484	1.772437368515101	-19.693047803006280
-6.2742	1.265512713848083	-4.956873352670034
-2.5097	0.913230941756339	-0.806257128073956
0	0.751125544464943	0.500000000000000
3.1371	0.645961493829006	1.526594842533555

Table 2: Numerical values E^{ref} and $\phi_E^{\text{ref}}(0)$ computed on a larger domain for different β.

the exact harmonic potential solution ($\beta = 0$)

$$\phi_0^{M,0}(x) = \frac{1}{\pi^{1/4}} e^{-x^2/2}.$$

The fixed point algorithm tolerance is $\varepsilon = 10^{-12}$ and the mesh size of the linear finite element method is $h = 10^{-3}$. Figures 35, 36 and 37 report the error on both the eigenvalue and eigenfunction at the origin depending on the right endpoint x_r, for the values $\beta = -6.2742$, $\beta = -2.5097$ and $\beta = 3.1371$, respectively.

Generally speaking, for a given case, all the algorithms converge with about the same number of iterations, independently of the boundary condition. We also note that, for negative values of β, the linearized ABCs lead to the same accuracy as the nonlinear ABCs (not reported here) for a similar computational time. In Figures 35 and 36, we only present the results for the Dirichlet boundary condition and SABC^{2,4}. For $\beta > 0$ (Figure 37), the linearized ABCs possess an accuracy at least equal to the one with SABC^{2,4}. We do not have any explanation about this fact. For $\beta = -6.2742$ (Figure 35), all the algorithms converge in 23 iterations. The ABCs improve the accuracy from a factor 10 compared with the Dirichlet boundary condition for $x_r = 1.5$, and almost 100 when $x_r = 2$, then for $x_r \geq 2.5$, all the boundary conditions have the same accuracy: 10^{-5}. The precision of the second-order ABC is slightly better than the fourth-order ABC. The reason is that these ABCs are formally derived, unlike the linear case. For $\beta = -2.5097$ (Figure 36), the convergence takes 14 iterations. The ABCs again provides a gain of precision compared with the Dirichlet boundary condition for x_r between 1.5 and 3.5, with a better accuracy for the second-order ABC (see the points $x_r = 3$ and $x_r = 2.5$ for example). For $\beta = 3.13712$, the situation is quite similar but requires 77 iterations to converge. Unlike, the two previous cases, the linearized ABCs give a slightly better accuracy than for the

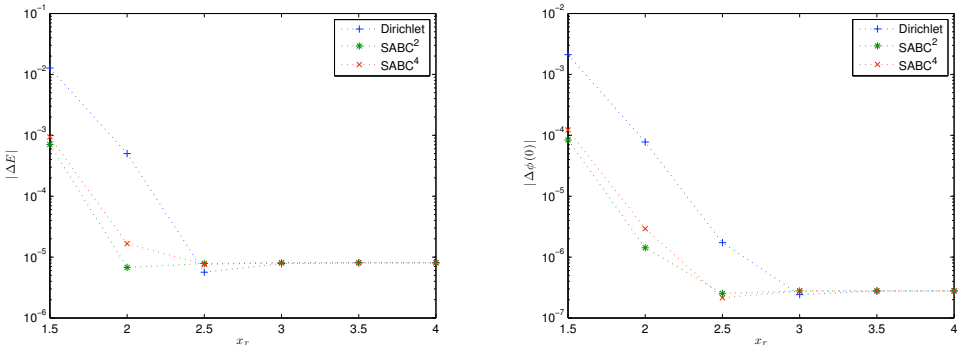

(a) Eigenvalue (b) Value of the eigenfunction at the origin

Figure 35: Errors ΔE and $\Delta\phi(0)$ for $\beta = -6.2742$.

original ABCs.

6. Conclusion

We have proposed some accurate and physically admissible absorbing boundary conditions for modeling linear and nonlinear stationary Schrödinger equations with variable potentials. Based on numerical schemes, these boundary conditions have been validated for many configurations including linear scattering and nonlinear ground-state computations.

Further extensions will include higher dimensional problems as well as variable mass Schrödinger equations among others. It might also be valuable to extent the presented work to systems of Schrödinger equations that arise as so-called *multiband effective mass approximations* (MEMAs) to model electronic states in modern semiconductor nanostructures, cf. [33, 34, 35]. Let us finally remark that applications to generalized Schrödinger equations could also be developed by adapting the methods developed in [2, 36].

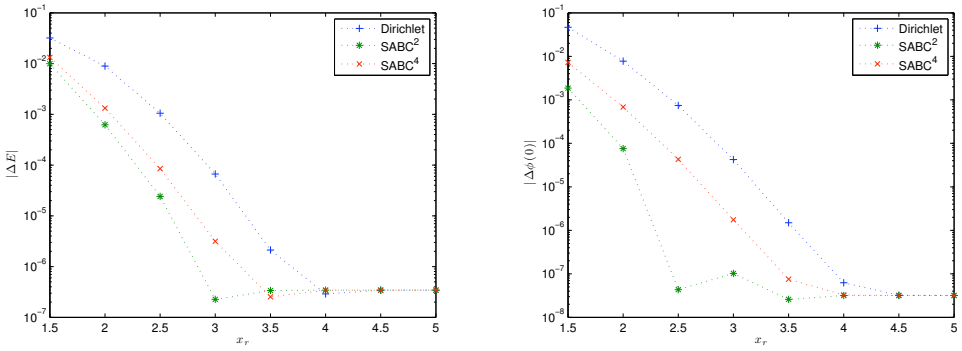

(a) Eigenvalue (b) Value of the eigenfunction at the origin

Figure 36: Errors ΔE and $\Delta\phi(0)$ for $\beta = -2.5097$.

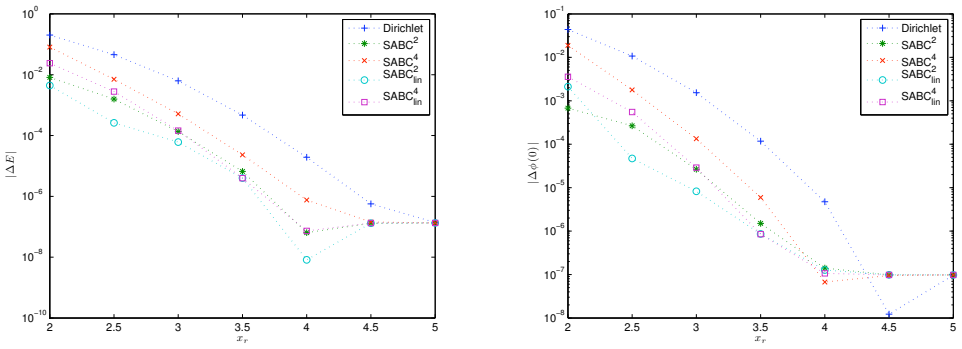

(a) Eigenvalue (b) Value of the eigenfunction at the origin

Figure 37: Errors ΔE and $\Delta\phi(0)$ for $\beta = 3.1371$.

[1] X. Antoine, A. Arnold, C. Besse, M. Ehrhardt, A. Schädle, A review of transparent and artificial boundary conditions techniques for linear and nonlinear Schrödinger equations, Commun. Comput. Phys. 4 (4) (2008) 729–796.

[2] X. Antoine, C. Besse, P. Klein, Absorbing boundary conditions for the one-dimensional Schrödinger equation with an exterior repulsive potential, J. Comput. Phys. 228 (2) (2009) 312–335.

[3] N. Ben Abdallah, P. Degond, P. A. Markowich, On a one-dimensional Schrödinger-Poisson scattering model, Z. Angew. Math. Phys. 48 (1) (1997) 135–155.

[4] A. Arnold, Mathematical concepts of open quantum boundary conditions, Trans. Theory Stat. Phys. 30 (2001) 561–584.

[5] C. Lent, D. Kirkner, The quantum transmitting boundary method, J. Appl. Phys. 67 (10) (1990) 6353–6359.

[6] D. Kirkner, C. Lent, S. Sivaprakasam, The numerical simulation of electron transmission through a two-dimensional quantum device by the finite element method, Int. J. Numer. Meth. Engineering. 29 (1990) 1527–1537.

[7] M. Ehrhardt, R. E. Mickens, Solutions to the discrete Airy equation: Application to parabolic equation calculations, J. Comput. Appl. Math. 172 (1) (2004) 183–206.

[8] M. Ehrhardt, A. Zisowsky, Fast calculation of energy and mass preserving solutions of Schrödinger-Poisson systems on unbounded domains, J. Comput. Appl. Math. 187 (1) (2006) 1–28.

[9] C. Moyer, Numerov extension of transparent boundary conditions for the Schrödinger equation in one dimension, Amer. J. Phys. 72 (3) (2004) 351–358.

[10] C. Moyer, Numerical solution of the stationary state Schrödinger equation using transparent boundary conditions, Comput. Sci. Engrg. 8 (4) (2006) 32–40.

[11] M. Ehrhardt, C. Zheng, Exact artificial boundary conditions for problems with periodic structures, J. Comput. Phys. 227 (14) (2008) 6877–6894.

[12] L. Burgnies, Mécanismes de conduction en régime ballistique dans les dispositifs électroniques quantiques, Ph.D. thesis, Université des Sciences et Technologies de Lille (1997).

[13] W. Frensley, Boundary conditions for open quantum driven far from equilibrium, Rev. Mod. Phys. 62 (1990) 745–791.

[14] P. Markowich, C. Ringhofer, C. Schmeiser, Semiconductor Equations, Springer, New-York, 1990.

[15] C. Schmeiser, Computational methods for semiclassical and quantum transport in semiconductor devices, Acta Numerica 3 (1997) 485–521.

[16] J. Yu, S. Dong, Exactly solvable potentials for the Schrödinger equation with spatially dependent mass, Phys. Lett. A 325 (3-4) (2004) 194–198.

[17] G. Chen, Z. Chen, Exact solutions of the position-dependent mass Schrödinger equation in D dimensions, Phys. Lett. A 331 (5) (2004) 312–315.

[18] M. Betcke, H. Voss, Stationary Schrödinger equations governing electronic states of quantum dots in the presence of spin-orbit splitting, Appl. Math. 52 (2007) 267–284.

[19] M. Taylor, Pseudodifferential operators, Vol. 34 of Princeton Mathematical Series, Princeton University Press, Princeton, N.J., 1981.

[20] M. Ehrhardt, Discrete transparent boundary conditions for Schrödinger-type equations for non-compactly supported initial data, Appl. Numer. Math. 58 (5) (2008) 660–673.

[21] I. M. Babuska, S. Sauter, Is the pollution effect of the FEM avoidable for the Helmholtz equation considering high wave numbers?, SIAM Review 42 (3) (2000) 451–484.

[22] J. Chazarain, A. Piriou, Introduction to the Theory of Linear Partial Differential Equations, North-Holland, Amsterdam/New-York, 1982.

[23] W. Bao, Q. Du, Computing the ground state solution of Bose-Einstein condensates by a normalized gradient flow, SIAM J. Sci. Comput. 25 (5) (2004) 1674–1697.

[24] H. Shao, Z. Wang, Arbitrarily precise numerical solutions of the one-dimensional Schrödinger equation, Comput. Phys. Commun. 180 (1) (2009) 1–7.

[25] E. Gross, Structure of a quantized vortex in boson systems, Nuovo Cimento 20 (3) (1961) 454–477.

[26] L. Pitaevskii, Vortex lines in an imperfect Bose gas, Soviet Physics JETP 13 (2) (1961) 451–454.

[27] W. Bao, The nonlinear Schrödinger equation and applications in Bose-Einstein condensation and plasma physics, in: Dynamics in Models of Coarsening, Condensation and Quantization, Vol. 9 of IMS Lecture Notes Series, World Scientific, 2007, pp. 215–255.

[28] W. Bao, W. Tang, Ground-state solution of Bose-Einstein condensate by directly minimizing the energy functional, J. Comput. Phys. 187 (1) (2003) 230–254.

[29] M. Dehghan, A. Taleei, A compact split-step finite difference method for solving the nonlinear Schrödinger equations with constant and variable coefficients, Comput. Phys. Commun. 181 (2010) 43–51.

[30] R. Thelwell, J. Carter, B. Deconinck, Instabilities of one-dimensional stationary solutions of the cubic nonlinear Schrödinger equation, J. Phys. A 39 (2006) 73–84.

[31] L. Carr, C. Clark, W. Reinhardt, Stationary solutions of the one-dimensional nonlinear Schrödinger equation. I. Case of repulsive nonlinearity, Phys. Rev. A 62 (2000) 063610.

[32] L. Carr, C. Clark, W. Reinhardt, Stationary solutions of the one-dimensional nonlinear Schrödinger equation. II. Case of attractive nonlinearity, Phys. Rev. A 62 (2000) 063611.

[33] A. Zisowsky, A. Arnold, M. Ehrhardt, T. Koprucki, Discrete transparent boundary conditions for transient $k \cdot p$-Schrödinger equations with

application to quantum-heterostructures, J. Appl. Math. Mech. 85 (11) (2005) 793–805.

[34] D. Klindworth, Discrete transparent boundary conditions for multiband effective mass approximations, Master's thesis, Technische Universität Berlin (2009).

[35] S. Odermatt, M. Luisier, B. Witzigmann, Bandstructure calculation using the $k \cdot p$ method for arbitrary potentials with open boundary conditions, J. Appl. Phys. 97 (2005) 046104.

[36] X. Antoine, C. Besse, V. Mouysset, Numerical schemes for the simulation of the two-dimensional Schrödinger equation using non-reflecting boundary conditions, Math. Comp. 73 (248) (2004) 1779–1799.